

1 **Title:** Ice Shell Structure and Composition of Ocean Worlds: Insights from Accreted Ice on
2 Earth

3 **Authors:** Natalie S. Wolfenbarger[†], Jacob J. Buffo[‡], Krista M. Soderlund[†], Donald D.
4 Blankenship[†]

5 [†]Institute for Geophysics, University of Texas at Austin, Austin, TX

6 [‡]Dartmouth College, Hanover, NH

7 **Corresponding Author:**

8 Natalie S. Wolfenbarger

9 J.J. Pickle Research Campus

10 University of Texas Institute for Geophysics

11 10100 Burnet Road

12 Austin, TX, 78759-8500, USA

13 818-919-9930

14 nwolfenb@utexas.edu

15

16 **Running Title:** Ice Shell Structure and Composition of Ocean Worlds

17

18 **Keywords:** ocean worlds, ice shell, marine ice, sea ice, fractionation, salinity

19

20 **Abstract:** Accreted ice retains and preserves traces of the ocean from which it formed. In this
21 work we study two classes of accreted ice found on Earth—frazil ice, which forms through
22 crystallization within a supercooled water column, and congelation ice, which forms through
23 directional freezing at an existing interface—and discuss where each might be found in the ice
24 shells of ocean worlds. We focus our study on terrestrial ice formed in low temperature gradient
25 environments (e.g., beneath ice shelves), consistent with conditions expected at the ice-ocean
26 interfaces of Europa and Enceladus, and highlight the juxtaposition of compositional trends in
27 relation to ice formed in higher temperature gradient environments (e.g., at the ocean surface).
28 Observations from Antarctic sub-ice-shelf congelation and marine ice show that the purity of
29 frazil ice can be nearly two orders of magnitude higher than congelation ice formed in the same
30 low temperature gradient environment (~0.1% vs. ~10% of the ocean salinity). In addition,
31 where congelation ice can maintain a planar ice-water interface on a microstructural scale, the
32 efficiency of salt rejection is enhanced (~1% of the ocean salinity) and lattice soluble impurities
33 such as chloride are preferentially incorporated. We conclude that an ice shell which forms by
34 gradual thickening as its interior cools would be composed of congelation ice, whereas frazil ice
35 will accumulate where the ice shell thins on local (rifts and basal fractures) or regional
36 (latitudinal gradients) scales through the operation of an “ice pump”.

37

38 **1. Introduction**

39 The ice shells of ocean worlds govern the feasibility of surface-ice-ocean exchange, thought to
40 be significant for supporting habitats within the sub-ice oceans (e.g., Soderlund *et al.* 2020). The
41 dynamic features and young surfaces of Europa and Enceladus provide compelling evidence that
42 their subsurface oceans are continuously interacting with their overlying ice shells (e.g., Howell
43 and Pappalardo 2018; Spencer *et al.* 2018). Because existing observations are mostly confined to

44 the surface, much attention has been directed towards the properties of the uppermost layer of the
45 ice shell, where the native ice could be modified by exogenic processes (Brown and Hand 2013).
46 Although observations of the surface provide important constraints on processes operating in the
47 subsurface (Zolotov and Shock 2001), the properties of the subsurface itself have received less
48 focus. Processes occurring at the ice-ocean interface, such as accretion, are likely responsible for
49 governing and modulating bulk properties of the ice shell (Zolotov and Shock 2001; Peddinti and
50 McNamara 2015; Buffo *et al.* 2020). Ice formed from the freezing of ocean water, referred to
51 here as accreted ice, might serve as a fingerprint of the ocean below, recording signals of
52 circulation (Langhorne and Robinson 1986), composition and salinity (Petrich and Eicken 2017),
53 and potentially life (Martin and McMinn 2018).

54
55 The ice-ocean interfaces of these alien worlds and the processes that mold and shape them may
56 be similar to those found in Earth's cryosphere. The extensive research conducted in pursuit of
57 understanding ice on Earth represents a foundation from which to build an understanding of ice
58 on other worlds. Previous work has leveraged sea ice as an analog to interpret surface features
59 and connect them to processes that may be operating within Europa's ice shell (Greeley *et al.*
60 1998), yet these authors advised caution in drawing direct analogies between the Earth and
61 Europa given their distinct environmental conditions. While recent works have revisited
62 terrestrial analogs to improve our understanding of potential ice-ocean interactions on other
63 worlds (e.g., Buffo *et al.* 2020; Schmidt 2020; Soderlund *et al.* 2020), only a small fraction of
64 this vast and relatively untapped resource has been leveraged to date.

65
66 In this work we demonstrate that ice forming in the low temperature gradient environment
67 beneath ice shelves can serve as a more relevant terrestrial analog than sea ice for ice forming
68 beneath the ice shells of ocean worlds, particularly Europa and Enceladus (Section 2). We
69 present two fundamental classes of accreted ice analogs: frazil ice and congelation ice (Section
70 3) and examine how their formation mechanisms influence bulk ice salinity at low temperature
71 gradients (Section 4). We identify where each class of accreted ice might form on icy ocean
72 worlds (Section 5), highlighting the implications for geophysical processes, bulk composition,
73 and astrobiology (Section 6).

74 75 **2. Physicochemical environments of Europa and Enceladus**

76 The exotic appearances of the ice shells of ocean worlds can sometimes mask the more mundane
77 reality that they are primarily composed of hexagonal water ice, the dominant ice on Earth.
78 Furthermore, at the ice-ocean interface, where accretion of ice occurs, the physical conditions
79 (e.g., composition, salinity, temperature, pressure) could be similar to those found in Earth's
80 polar regions. Table 1 depicts the observational and modeled constraints on the conditions at the
81 ice-ocean interfaces of Europa and Enceladus and demonstrates their similarity to Earth.

82

83

84

85

86 **TABLE 1.** Constraints on the conditions at the ice-ocean interfaces of Earth, Europa, and
 87 Enceladus from observations and models. Two possible ocean compositions are presented for
 88 Europa: (i) a sulfate-dominated ocean and (ii) a carbonate-dominated ocean. The estimates of ice
 89 thickness for Europa refer to estimates from crater and thermodynamic analyses. The pressure
 90 and temperature estimates are derived from the ice thickness ranges presented here and assume
 91 pure water ice at a density of 917 kg/m³ and a freshwater ocean.
 92

Parameter	Europa	Enceladus	Earth	References
Composition (Dominant Ions)	(i) SO ₄ ²⁻ , Mg ²⁺ , Na ⁺ , Cl ⁻ (ii) HCO ₃ ⁻ , Na ⁺ , SO ₄ ²⁻ , Mg ²⁺	Na ⁺ , Cl ⁻ , HCO ₃ ⁻ , CO ₃ ²⁻	Cl ⁻ , Na ⁺ , Mg ²⁺ , SO ₄ ²⁻	Zolotov and Shock (2001); Zolotov (2007); Glein <i>et al.</i> (2015); Glein <i>et al.</i> (2018); Postberg <i>et al.</i> (2018); Fox-Powell and Cousins (2021); Melwani Daswani <i>et al.</i> (2021)
Salinity (Constrained by Geochemical Models)	12 ppt*	2–20 ppt	N/A	Zolotov and Shock (2001); Zolotov (2007)
Salinity (Constrained by Observation)	>5 ppt	4–40 ppt	35 ppt (standard)	Schilling <i>et al.</i> (2007); Millero <i>et al.</i> (2008); Postberg <i>et al.</i> (2009); Hsu <i>et al.</i> (2015)
Floating Ice Thickness	3–38 km	2–50 km	0–3 km	Billings and Kattenhorn (2005); less <i>et al.</i> (2014); McKinnon (2015); Čadek <i>et al.</i> (2016); Čadek <i>et al.</i> (2019)
Pressure	3.6–46 MPa	0.2–5.2 MPa	0.1–27 MPa	
Pressure-Melting Temperature	269–273 K	273 K	271–273 K	

93 *Note that Kargel (1991) obtained models predicting peritectic and eutectic European oceans

94 The composition and salinity of accreted ice serves as a signature of the environment in which it
 95 formed (Zolotov and Kargel 2009; Buffo *et al.* 2020). Although the compositions of the
 96 subsurface oceans on Europa and Enceladus have not been measured directly, constraints exist
 97 from theory and interpretations of data collected by both space-based and Earth-based platforms
 98 (e.g., Zolotov and Shock 2001; Postberg *et al.* 2011). Because the composition of the source
 99 water influences the properties of the ice (i.e., phase behavior governs brine volume fraction
 100 which influences thermophysical, dielectric, and mechanical properties) (Petrich and Eicken
 101 2017), it should be considered when evaluating the relevance of terrestrial accreted ice as an
 102 analog.

103 Measurements of the Enceladus plume material by *Cassini* represent the only in situ observations
 104 of apparent oceanic material in the outer solar system (Glein *et al.* 2018). These observations,
 105 coupled with geochemical models (Zolotov 2007; Glein *et al.* 2015), suggest that the Enceladan
 106 ocean is highly alkaline and dominantly composed of sodium and chloride (Glein *et al.* 2018;
 107 Postberg *et al.* 2018). Assuming the plume material represents a relatively unfractionated (i.e.,
 108 flash-frozen) sample of oceanic material (Fox-Powell and Cousins 2021), the salinity of the
 109 Enceladan ocean could be up to ~20 ppt—only slightly less than Earth’s (~35 ppt) (Postberg *et*
 110 *al.*, 2011)—although later work argues for an upper limit salinity of ~40 ppt based on the
 111 detection of silica nanoparticles in the plume material (Hsu *et al.* 2015). However, recent ocean
 112 modeling studies demonstrated that low salinity layers could be present at the ice-ocean interface

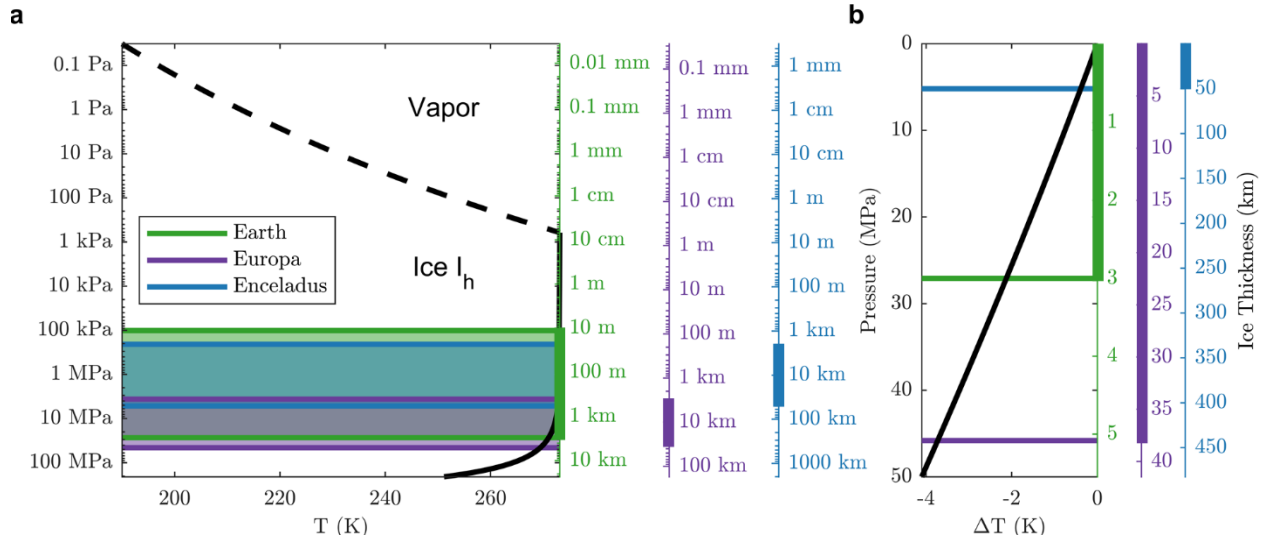
113 near the poles which would imply that the salinity inferred from plume material may be lower
114 than the bulk ocean salinity (Lobo *et al.* 2021; Zeng and Jansen 2021).

115 Although a plume sample remains elusive for Europa, geochemical models of Europa's ocean
116 chemistry have attempted to constrain the dominant species using observations of Europa's
117 surface and atmosphere. For example, the Europa K1a model of Zolotov and Shock (2001) was
118 tuned by Earth-based observations of chemical species detected in Europa's tenuous atmosphere
119 (Brown 2001). This model suggested that Europa's ocean composition is broadly comparable to
120 that of the Earth's, where the dominant ionic species are sulfate, magnesium, sodium, and
121 chloride. Other geochemical models identify similar dominant species, although their relative
122 abundance (NaCl-dominated vs. MgSO₄-dominated) remains the subject of debate (Kargel *et al.*
123 2000; Zolotov 2008; Zolotov and Kargel 2009). Results from a more recent model suggest that a
124 carbonate dominated European ocean is also possible (Melwani Daswani *et al.* 2021). Early
125 interpretations of *Galileo* NIMS data were consistent with the presence of hydrated sulfate or
126 carbonate salts in regions associated with resurfacing (McCord *et al.* 1998; McCord *et al.* 1999).
127 Later analysis by Carlson *et al.* (2005) suggested that the signature could instead be attributed to
128 hydrated sulfuric acid. This would also explain the apparent enhancement observed on the
129 trailing hemisphere, where the surface is highly irradiated and bombarded by Iogenic sulfur.
130 Higher spectral resolution observations acquired by Earth-based platforms were able to identify
131 features associated with magnesium sulfate salts but found that they were confined to the trailing
132 hemisphere and spatially correlated with sulfuric acid (Brown and Hand 2013). Brown and Hand
133 (2013) used the spatial correlation of the magnesium sulfate with radiation products to argue that
134 sulfate salts are a radiation product and that the ice shell and ocean are dominantly composed of
135 chloride salts, which have no distinct spectral feature in the near-infrared. These results were
136 supported by additional Earth-based observations, which were able to confirm that acid-
137 dominant components were concentrated along the trailing hemisphere and salt-dominant
138 components were associated with endogenous surface features (Fischer *et al.* 2015).
139 Additionally, because the salt-dominant component lacked spectral features consistent with
140 hydrated sulfate minerals, the authors proposed the spectrum may instead be associated with
141 chloride evaporite deposits. Laboratory experiments have demonstrated that when sodium
142 chloride is exposed to conditions similar to those expected at Europa's surface, it darkens into a
143 color consistent with that observed across Europa's surface, particularly in features thought to be
144 associated with material from the sub-ice ocean (Hand and Carlson 2015). Recent observations
145 of Europa's surface with the *Hubble Space Telescope* revealed a spectral feature consistent with
146 irradiated sodium chloride that was again highly correlated with endogenous features (Trumbo *et al.*
147 2019). These laboratory, Earth-based, and space-based observations collectively indicate that
148 chloride salts are being entrained in the ice shell. Similar to the Earth and Enceladus, chloride
149 may represent an important component of Europa's ocean composition.

150 Although measurements of Europa's induced magnetic field by the *Galileo* magnetometer
151 support the existence of a global subsurface ocean; constraining the salinity of the ocean from
152 these measurements is a challenge as the signal is a convolution of electrical conductivity and
153 ice/ocean thicknesses. Gravitational measurements from *Galileo* flybys provide an upper limit of
154 ~200 km to the thickness of the ice/ocean layer (Anderson *et al.* 1998). Using this thickness
155 constraint and a minimum value of 0.7 for the normalized amplitude of the induced dipole
156 moment relative to the primary field, Zimmer *et al.* (2000) were able to estimate a minimum

157 ocean conductivity of 0.072 S/m. Later work by Schilling *et al.* (2007) further constrained the
158 parameter space to obtain a minimum conductivity of 0.5 S/m for a 100 km ocean. For terrestrial
159 seawater at 0 °C, this translates to a practical salinity (PSS-78) of ~5. Hand and Chyba (2007)
160 use the induced magnetic field amplitude of 0.97 obtained by Schilling *et al.* (2004) to argue for
161 an ice shell less than 15 km thick overlying an ocean of conductivity that could range from 3 S/m
162 (practical salinity of ~36 at 0 °C) to 23 S/m (practical salinity undefined) More recent work by
163 Vance *et al.* (2021b) argues that the reduction in electrical conductivity with decreasing
164 temperature could raise these salinity estimates for colder oceans associated with thicker ice
165 shells. This suggests, because of the broad parameter space of possible ocean salinities, a valid
166 ocean analog could span in salinity from brackish to hypersaline.

167 The surfaces of icy ocean worlds are directly exposed to the vacuum of space and have measured
168 temperatures ranging from approximately 86 K to 132 K on Europa (Spencer *et al.*, 1999) and 32
169 K up to 145 K on Enceladus (Spencer *et al.* 2006). At the south pole of Enceladus, the
170 temperature approaches 200 K near a set of linear features, referred to as tiger stripes, which are
171 spatially correlated with the plumes observed by *Cassini* and are thought to serve as a conduit to
172 the subsurface ocean (Spencer *et al.* 2018; Hemingway *et al.* 2020). The conditions at depth,
173 however, could be relatively mild. The equivalent of one Earth atmosphere of pressure translates
174 to ~100 m of ice on Europa and ~1 km of ice on Enceladus (Fig. 1a). This suggests the near-
175 vacuum conditions at the surface of these bodies becomes irrelevant at relatively shallow depths,
176 well-below the hypothesized ice shell thicknesses of Europa and Enceladus (Table 1). The
177 pressure ranges expected beneath these ice shells are consistent with what is expected beneath
178 floating ice on Earth, which can be up to a few kilometers thick (Table 1, Fig. 1). The melting
179 temperature of ice does not vary significantly with pressure for ice shell thicknesses of
180 approximately 1 m to a few kilometers on Europa and 10 m to tens of kilometers on Enceladus.
181 This suggests that for both Europa and Enceladus, neglecting the influence of impurities, the
182 temperature at the ice-ocean interface is likely to be depressed by only a few degrees (~3 K
183 beneath a 30 km ice shell on Europa, ~0.5 K beneath a 50 km ice shell on Enceladus). Note that
184 although the influence of pressure on melting temperature is minor, it is critical to driving “ice
185 pumps” beneath ice shelves on Earth, a basal ice redistribution process introduced and further
186 discussed in Section 3.2. The pressure-melting temperature represents an upper limit for the
187 temperature at the ice-ocean interface since impurities within the ocean can further reduce the
188 equilibrium temperature.



189

190 **FIG. 1.** Pressure at the ice-ocean interface for the range of ice shell thicknesses on Earth (green
 191 axis), Europa (purple axis), and Enceladus (blue axis) represented **(a)** logarithmically across the
 192 entire stable region of ice I_h and **(b)** linearly across the range of pressures expected at the ice-
 193 ocean interfaces of these worlds. The Earth axis does not include the effect of atmospheric
 194 pressure, hence the minimum pressure-equivalent thickness of 10 m. The dashed black curve
 195 depicts the phase boundary between Ice I_h and water vapor, and the solid black curve depicts the
 196 phase boundary between Ice I_h and liquid water. The range of floating ice thickness for each
 197 body, specified in Table 1, is represented by the shaded region in (a). The colored lines depict the
 198 upper and lower bounds of ice thickness. Only the upper bound ice thickness is included in (b).
 199 The density of ice is taken to be constant at 917 kg/m³.

200

201 Freezing point depression is a mechanism often invoked to explain the presence of liquid water
 202 in otherwise cryogenic environments (Toner *et al.* 2014; Hammond *et al.* 2018). For an ideal
 203 solution with low concentrations of impurities, freezing point depression is dependent upon the
 204 concentration of dissolved impurities, but not their composition. As the eutectic point is
 205 approached, this colligative assumption breaks down and composition becomes relevant to the
 206 freezing point depression. For the range of plausible salinities and ice shell thicknesses
 207 hypothesized for Europa, this implies the temperature at the ice-ocean interface could range from
 208 the pressure-melting point to the eutectic point of a salt solution. For a sodium chloride ocean,
 209 the maximum freezing point depression would be ~21 K at a concentration of 232 ppt
 210 (Drebushchak *et al.* 2019), whereas for a magnesium sulfate ocean, the maximum corresponds to
 211 only ~4 K at a concentration of 174 ppt (Pillay *et al.* 2005). Ammonia, initially implicated in
 212 promoting resurfacing processes at Enceladus (Squyres *et al.* 1983), can depress the freezing
 213 point of water by almost 100 K at a concentration of 354 ppt (Leliwa-Kopystyński *et al.* 2002);
 214 however, only trace amounts were detected in the Enceladus plume material (Waite *et al.* 2009;
 215 Waite *et al.* 2017; Fox-Powell and Cousins 2021). If the plume observation is representative of
 216 the concentration of ammonia within the subsurface ocean, it would amount to a freezing point
 217 depression on the order of a degree. The composition and concentration of impurities, in addition
 218 to the overburden pressure, defines where multiphase systems can exist within the ice shell

219 (Hammond *et al.* 2018)—creating the opportunity for complex reactive transport processes
220 important to the habitability of these worlds (Kalousová *et al.* 2014; Buffo *et al.* 2020; Hesse *et*
221 *al.* 2020).

222 3. Terrestrial Accreted Ice

223 Although the physicochemical environments of Europa and Enceladus may share similar
224 characteristics to ice-ocean interfaces on Earth, a critical distinction between the ice-ocean
225 interfaces of ocean worlds in the outer solar system and Earth involves the temporal and spatial
226 scales of processes operating at that interface (Vance *et al.* 2021a). Timescales of freezing
227 processes beneath the ice shells of ocean worlds are likely orders of magnitude slower than sea
228 ice on Earth (i.e., sea ice growth occurs on seasonal cycles, whereas the ice shells of ocean
229 worlds are potentially the product of over a hundred million years of accretion and ablation). The
230 temperature gradient at the ice-ocean interface is an important consequence of these vastly
231 different temporal and spatial scales. If the ice is actively thickening and in a conductive thermal
232 regime, the temperature profile is approximately linear throughout the shell, and the magnitude
233 of the temperature gradient is governed by the thickness of the ice layer and temperature at the
234 surface and base of the ice layer (Thomas 2017). As such, the thick ice shells of ocean worlds are
235 subject to lower temperature gradients and freezing rates than experienced by sea ice on Earth
236 (Table 2). Furthermore, as the ice shell approaches equilibrium thickness, the growth rates
237 should decrease to zero. Therefore, we consider the estimated freezing rates for Europa and
238 Enceladus in Table 2 to represent upper bounds, which are notably over an order of magnitude
239 lower than sea ice growth rates measured on Earth. Although sea ice is one of the most
240 ubiquitous and most studied forms of accreted ice on Earth, we propose that there are other
241 forms of ice which may represent more relevant analogs for ice accreting at the ice-ocean
242 interface of ocean worlds.

243

244

245

246

247

248

249

250

251

252

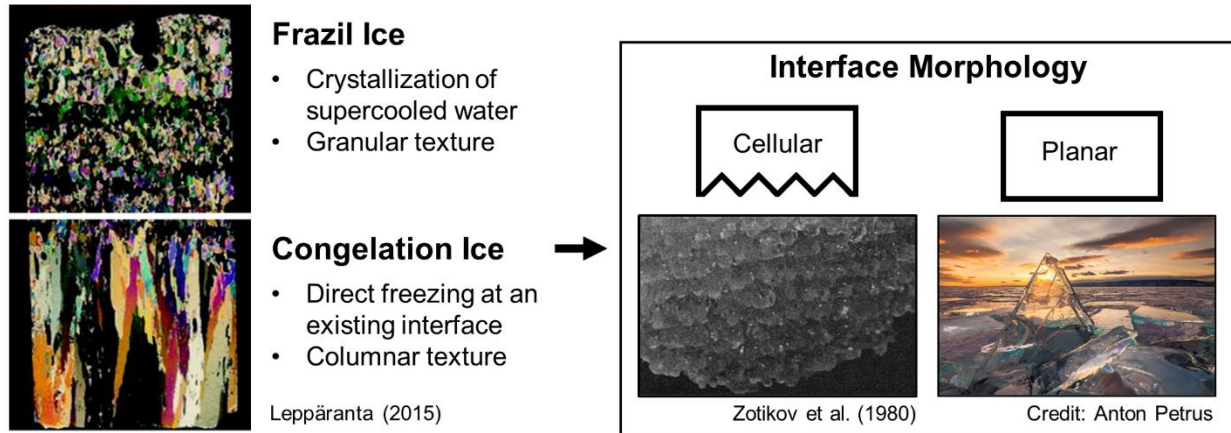
253

254

255 **TABLE 2.** Estimates of ice shell growth rates for Europa and Enceladus compared to measured
 256 sea ice growth rates on Earth. Growth rates are expressed in terms of the published units and in
 257 cm/s for direct comparison. All modeled freezing rates for Europa and Enceladus neglect the
 258 influence of salts and thus may be higher than reality.

	v	$v \times 10^6$ (cm/s)	Source
Sea Ice	0.7 – 1.7 cm/day	8.1 – 20	Nakawo and Sinha (1981)
Sea Ice	0.15 – 2.29 cm/day	1.7 – 27	Souchez <i>et al.</i> (1988)
Sea Ice	1.2 – 4.5 cm/day	14 – 52	Legendre <i>et al.</i> (1991)
Sea Ice	0.03 cm/hr – 0.38 cm/hr	8.3 – 105	Melnikov (1995)
Sea Ice (Nominal Max)	1.5 – 3 cm/day	17 – 35	Shokr and Sinha (2015)
Europa	150 km ocean freezing in 100 Myr	0.005	Pappalardo <i>et al.</i> (1998)
Europa	30 km freezing in 7×10^6 yr	0.014	Mitri and Showman (2005)
Europa	100 km ocean freezing in 62 Myr	0.005	Quick and Marsh (2015)
Europa	Increase from 5.67 km/Myr to 8.22 km/Myr due to merging of convective cells	0.018 – 0.026	Peddinti and McNamara (2019)
Europa	30 km freezing in 1.5 Myr ($\dot{\epsilon} = 1 \times 10^{-10} \text{ s}^{-1}$) 5 km freezing in 165 kyr ($\dot{\epsilon} = 3 \times 10^{-10} \text{ s}^{-1}$)	0.063 – 0.096	Green <i>et al.</i> (2021)
Enceladus	40 km ocean freezing in 30 Myr	0.004	Roberts and Nimmo (2008)
Enceladus	<few mm/yr to maintain topographic anomalies	<0.01	Čadek <i>et al.</i> (2019)
Enceladus	~km/Myr freezing rate required to maintain steady state	<0.01	Kang <i>et al.</i> (2021)

259
 260 Ice which accretes beneath the thick ice shelves of Antarctica forms in a significantly lower
 261 temperature gradient environment than sea ice and could approach growth velocities relevant to
 262 the ice-ocean interfaces beneath the ice shells of ocean worlds. In this work, we adopt the genetic
 263 terminology of Tison *et al.* (1998) and focus our study on two classes of accreted ice found
 264 beneath ice shelves: frazil ice and congelation ice (Fig. 2). Although naturally accreted ice is
 265 rarely composed entirely of frazil or congelation ice, these broad classifications facilitate
 266 discussions of bulk ice properties in the context of their formation mechanisms and will allow us
 267 to examine how each might influence the bulk salinity of the ice shells of ocean worlds.
 268



269

270 **FIG. 2.** Genetic classification of accreted ice and characteristics of the microstructural interface
 271 morphology for congelation ice.

272

273 3.1. Frazil and Congelation Ice

274 Ice that crystallizes within a supercooled water column, as opposed to at a solid interface, is
 275 referred to as frazil ice. Frazil ice is formed in the presence of turbulent water which has been
 276 supercooled by tenths to hundredths of a degree (Weeks and Ackley 1986; Mager *et al.* 2013;
 277 Robinson *et al.* 2019), where increased supercooling generally promotes increased frazil
 278 production (Ettema *et al.* 1984). There are a number of mechanisms in nature that can promote
 279 supercooling and thus the production of frazil ice. Examples of such mechanisms include the
 280 adiabatic rise of water masses to a lower-pressure environment and double diffusion occurring
 281 between two adjacent water bodies at different temperatures and salinities (see Mager *et al.*
 282 2013). Ice crystals formed from collisions of larger ice crystals, the refreezing of spray, or snow
 283 can serve as nucleation sites for frazil ice crystals (Osterkamp 1977). It was long believed that
 284 foreign particles, such as organic matter, could serve as nucleation sites for frazil, but no
 285 experimental or field observations have demonstrated that this is possible at the degrees of
 286 supercooling observed in nature (<1 °C) (Daly 1984; Robinson *et al.* 2019). Turbulence is also
 287 necessary to promote secondary nucleation, responsible for generating meaningful quantities of
 288 frazil crystals (Ettema *et al.* 1984). Because frazil ice forms from individual crystals which can
 289 nucleate independent of each other, it has no preferred orientation and a granular texture (Fig. 2).
 290 Once a stable frazil ice layer has formed, congelation ice growth can occur.

291 Congelation ice refers to ice produced by the direct freezing of water at an existing ice interface,
 292 driven by conductive heat losses (Weeks and Ackley 1986). In congelation ice, the
 293 microstructural morphology of the ice-water interface (e.g., planar, cellular, dendritic) is highly
 294 dependent on the purity of the source water and the growth velocity (Harrison and Tillier 1963;
 295 Lofgren and Weeks 1969; Wettlaufer 1992; Wettlaufer 1998). Ultimately, the microstructural
 296 morphology of the ice-ocean interface is related to the phenomenon of constitutional
 297 supercooling (Harrison and Tillier 1963; Eicken 2003), originally proposed and studied in the
 298 field of metallurgy (Rutter and Chalmers 1953; Jackson 2004). Constitutional supercooling refers
 299 to supercooling that occurs in advance of the freezing front. The role of constitutional
 300 supercooling in congelation ice growth is critical to governing its substructure and in turn its

301 properties (Eicken 2003; Weeks 2010; Petrich and Eicken 2017). Rejection of impurities locally
302 enhances the concentration and depresses the freezing point at the interface, promoting
303 supercooling ahead of the interface. If perturbations occur in the presence of constitutional
304 supercooling, the supercooled fluid serves as a heat sink that promotes further growth, forming
305 cells or dendrites. In the absence of this supercooled layer, small perturbations in the interface
306 morphology are not energetically favorable and a planar interface remains stable.

307 Characteristics of the interface are significant to the efficiency of impurity incorporation in ice
308 (Nagashima and Furukawa 1997). A planar interface is more efficient at rejecting impurities,
309 whereas a cellular interface retains impurities through the entrapment of brine between cells
310 (Osterkamp and Weber 1970; Eicken 2003; Weeks 2010; Petrich and Eicken 2017). For the
311 growth rates typical of sea ice on Earth (Table 2), it has been demonstrated that congelation ice
312 forming from seawater will always result in the development of a cellular interface (Wetlaufer
313 1992). Congelation ice is typically characterized by a columnar texture, where crystals
314 preferentially elongate parallel to the direction of the temperature gradient (Harrison and Tiller
315 1963; Tison *et al.* 1998). In low salinity environments, such as freshwater lakes, constitutional
316 supercooling during freezing is minimal and the morphology of the microstructural interface can
317 remain planar for higher growth velocities than it would for seawater (Leppäranta 2015).

318 3.2. Marine Ice and Sub-Ice-Shelf Congelation Ice

319 Marine ice is specific to frazil ice that collects and consolidates beneath ice shelves or within ice
320 shelf rifts characterized by a low temperature gradient environment. The formation of marine ice
321 is generally thought to occur in two phases, defined by Tison *et al.* (2001) as (1) the frazil ice
322 phase and (2) the consolidation phase. The frazil phase encompasses the formation and
323 accumulation of frazil ice crystals beneath the ice shelf. These crystals preferentially form and
324 collect where the ice draft thins rapidly—features such as inverted channels, rifts, or crevasses
325 beneath the ice shelf (Tison *et al.* 1993; Khazendar *et al.* 2001; Khazendar and Jenkins 2003).
326 The consolidation phase involves the buoyancy-driven compaction of accumulated frazil
327 crystals. In this phase, crystals agglomerate and collect, forming a permeable layer. As more
328 frazil accumulates, buoyant pressure builds up at the ice-water interface, compressing the layer
329 and forcing out interstitial water, reducing the brine volume fraction. The bulk density of the ice-
330 brine system is thus counter-intuitively reduced by compaction. At a certain stage in the
331 consolidation phase, the ice becomes impermeable and any remaining brine is trapped in the ice
332 as inclusions at triple-junctions and along grain boundaries (Moore *et al.* 1994). The final stage
333 of consolidation involves the freezing of remaining interstitial water through congelation growth,
334 analogous to the incorporation of frazil ice layers beneath growing sea ice known as platelet ice.
335 Unlike platelet ice, this interstitial congelation growth occurs at a much slower rate due to the
336 insulation from atmospheric thermal forcing by overlying glacial ice. The lower unconsolidated
337 portion of the marine ice layer is a hydraulically connected region that can extend from tens of
338 meters up to ~100 m from the base of the ice shelf (Craven *et al.* 2009). The formation of marine
339 ice beneath ice shelves is part of a process that has been referred to as an “ice pump”, where the
340 pressure dependence of the freezing point supports the operation of a continuous cycle involving
341 the melting of ice at depth and the accretion of ice at a more shallow location (Lewis and Perkin
342 1986). The term marine ice is sometimes broadly applied to ice that forms beneath ice shelves.
343 Here, however, we distinguish between marine ice and sub-ice-shelf congelation ice to
344 emphasize the distinct formation mechanisms between these forms of accreted ice.

345 Because the ice-ocean interface beneath ice shelves is fairly insulated from atmospheric forcing
346 (i.e., the ocean is shielded from frigid air temperatures by hundreds of meters of ice), the
347 formation of congelation ice at the base of an ice shelf is rare (Fig. 4); however, it has been
348 observed beneath certain ice shelves in Antarctica (Gow and Epstein 1972; Zotikov *et al.* 1980;
349 Souchez *et al.* 1991). A simple model to predict the formation of congelation ice beneath an ice
350 shelf was proposed by the Ross Ice Shelf Project (RISP) and summarized by Neal (1979). When
351 water at the pressure-melting temperature flows in the direction of increasing ice shelf thickness,
352 it must dissipate heat to remain at the pressure-melting temperature. Under conditions where the
353 thickness gradient and flow speed are such that the sensible heat conduction to the overlying ice
354 layer exceeds that which must be dissipated at the boundary layer to maintain the pressure-
355 melting temperature, bottom freezing will occur (Neal 1979). The J-9 Ross Ice Shelf core
356 represents a unique and valuable sample of congelation ice acquired at a depth of ~400 m within
357 a zone of bottom freezing (Zotikov *et al.* 1980). The published sample is uniquely well-
358 characterized for sub-ice-shelf congelation ice and includes measurements of salinity, grain size,
359 texture, and freezing rate. The freezing rate estimate was obtained from an observed transition in
360 growth conditions at the bottom 2 cm, which was attributed to localized melting caused by a
361 drilling expedition the prior year (Zotikov *et al.* 1980). The estimate was validated by a simple
362 heat transfer calculation (Zotikov *et al.* 1980) and represents the only estimate of sub-ice-shelf
363 congelation ice growth rate obtained through direct inspection of a sample of the basal accreted
364 ice. Congelation ice can also form beneath ice shelves experiencing high rates of surface ablation
365 (e.g., locations with strong katabatic winds) (Souchez *et al.* 1991).
366

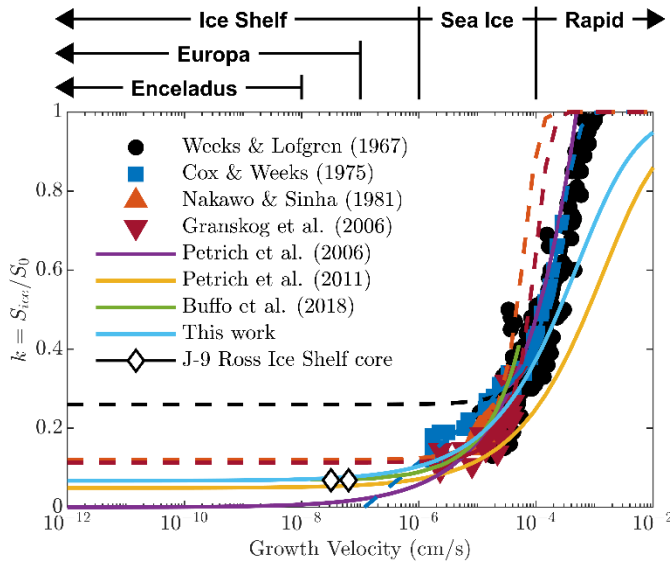
367 4. Salinity of Accreted Ice from Experiments and Ice Cores

368 We review published studies characterizing the bulk salinity of accreted ice to develop an
369 understanding for how salt entrainment processes might scale to the ice shells of ocean worlds.
370 As ice forms, salts are rejected from the crystal lattice to the grain boundaries as brine. Select
371 impurities, specifically chloride, fluoride, ammonium, and acids (H⁺), are soluble within the ice
372 lattice and are accommodated as defects within the ice crystal. The total concentration of salts in
373 ice, including both those accommodated within the lattice and those along grain boundaries, is
374 referred to as the bulk salinity (Hunke *et al.* 2011). Because the efficiency of salt entrainment in
375 ice is correlated to the ice growth velocity, we explore relationships modeling the bulk salinity of
376 ice as a function of growth velocity and show that only salt entrainment in the slowest growth
377 velocity regime is relevant to the bulk salinity of the ice shells of Europa and Enceladus. We then
378 focus our study on ice cores collected in environments which represent ice-ocean accretion
379 within this regime.

380 4.1. Congelation Ice across Growth Regimes

381 The partitioning of salt into ice, S_{ice} , from ocean water of salinity, S_0 , can be represented by the
382 effective solute distribution coefficient, $k(v) = S_{ice}/S_0$, which is a function of ice growth
383 velocity (Burton *et al.* 1953; Weeks and Lofgren 1967). Although models for the effective solute
384 distribution coefficient do not directly represent the physics of sea ice desalination as it is
385 understood today (Notz and Worster 2009), existing models fit the data well for both natural and
386 artificial ice over a range of freezing rates relevant to sea ice (Fig. 3). Parameterizations of salt
387 partitioning based on growth velocity represent a computationally inexpensive approach to

388 augment simple freezing models that do not directly model ice desalination processes.
 389 Furthermore, representing the salinity of ice as a fraction of ocean salinity allows salt
 390 entrainment in ice to be parameterized independent of the source water salinity. Even though
 391 more complex numerical models of ice desalination processes exist (Griewank and Notz 2013;
 392 Buffo *et al.* 2018; Wells *et al.* 2019), effective solute distribution coefficients are invaluable for
 393 certain planetary applications where high-resolution salinity profiles are not needed and
 394 properties of the ocean are poorly constrained.



395
 396 **FIG. 3.** Summary of relationships representing the effective solute distribution coefficient, $k =$
 397 S_{ice}/S_0 , as a function of ice growth velocity. The markers represent data points from
 398 experimental or field data. Solid lines through data points represent least squares fits of the data
 399 to published models for the solute distribution coefficient, where dashed lines represent
 400 extensions of the model beyond the available data range. The green curve is a smoothed
 401 representation of multiple runs of the mushy-layer model of Buffo *et al.* (2018), assuming a
 402 critical porosity inferred from the salinity of the J-9 core from Ross Ice Shelf, Antarctica. The
 403 light blue curve represents the model presented in Eq. 6.

404 At growth velocities above those naturally occurring on Earth (Fig. 3), ice experiences minimal
 405 fractionation ($k \approx 1$) upon freezing, implying that it serves as a relatively unaltered chemical
 406 fingerprint of the source water. This rapid freezing regime would include processes occurring at
 407 or near the surface at Europa and Enceladus such as the flash freezing of brine infiltrating porous
 408 ice at the surface or plume material which is frozen as it ascends through the fractured ice shell
 409 from a subsurface reservoir below (McCord *et al.* 2002; Schmidt *et al.* 2011; Thomas *et al.* 2017;
 410 Fox-Powell and Cousins 2021). Published measurements of sea ice growth rates span from
 411 approximately 10^{-6} to 10^{-4} cm/s (Table 2). Salt partitioning in this regime has been
 412 characterized using both natural (Nakawo and Sinha 1981; Granskog *et al.* 2006) and artificial
 413 (Weeks and Lofgren 1967; Cox and Weeks 1975) samples of congelation ice. Studies of natural
 414 sea ice samples are more challenging due to the difficulties in obtaining samples and the
 415 uncertainties in natural growth rates. The dataset of Nakawo and Sinha (1981) is particularly

416 valuable because of the high sampling frequency of ice salinity and temperature they obtained
417 over the growth season that produced nearly continuous profiles of ice salinity and growth rate.
418 Although growth velocities for the sea ice regime and above are not directly applicable to
419 accretion occurring at the ice-ocean interface of ocean worlds (Fig. 3), it represents the regime
420 where the effective solute distribution coefficient is most sensitive to growth velocity and where
421 more significant variations in bulk ice shell salinity might occur.

422 At a certain stage in growth, the salinity profile of the ice no longer evolves in time due to
423 progressive brine drainage. This salinity has been referred to as the stable salinity (Nakawo and
424 Sinha 1981; Petrich *et al.* 2006) or steady-state salinity (Petrich *et al.* 2011). The natural
425 congelation ice samples of Nakawo and Sinha (1981) in Fig. 3 are thought to be representative of
426 this stable salinity and as such fall below the experimental data, which was not given sufficient
427 time to reach this steady-state condition. The Baltic sea ice samples of Granskog *et al.* (2006) in
428 Fig. 3 represent the stable salinity of ice formed from a lower salinity source water. These data
429 suggest that a lower salinity source water may enhance the efficiency of salt rejection, possibly
430 due to a change in interface morphology (Granskog *et al.* 2006). Their data are consistent with
431 those of Weeks and Lofgren (1967), which included samples formed from low salinity source
432 waters.

433 Because salt in ice is predominantly trapped interstitially as brine, the steady-state salinity is
434 thought to be coupled to a critical porosity ($\sim 5\%$) below which ice is thought to be impermeable
435 to brine transport (Golden *et al.* 1998; Golden *et al.* 2007). The critical porosity is typically a
436 prescribed parameter in numerical models of sea ice desalination (Petrich *et al.* 2011; Griewank
437 and Notz 2013; Buffo *et al.* 2018; Wells *et al.* 2019; Buffo *et al.* 2020) and governs the finite ice
438 salinity that the model asymptotically approaches as the growth velocity approaches zero (i.e.,
439 the system reaches equilibrium) (Fig. 3). The distribution coefficient associated with this limit
440 has been referred to as the effective equilibrium distribution coefficient, k_{eq} (Burton *et al.* 1953;
441 Weeks and Lofgren 1967) and would represent the bulk salinity of congelation ice as the growth
442 velocity approaches zero. Other sea ice desalination models do not explicitly impose a critical
443 porosity, but instead use permeability-porosity relationships that represent a percolation
444 threshold as a significant reduction in permeability which occurs as the critical porosity is
445 approached (Petrich *et al.* 2006; Buffo *et al.* 2021a). Figure 3 demonstrates that at the growth
446 velocities predicted for the ice shells of ocean worlds, the effective equilibrium solute
447 distribution coefficient should govern the bulk salinity of the ice shell.

448 4.2. Low Temperature Gradient Accreted Ice

449 For ocean worlds, we are interested in the accretion of ice in low temperature gradient
450 environments characterized by growth velocities within the ice shelf regime ($< 10^{-6}$ cm/s),
451 where $k \approx k_{eq}$ (Fig. 3). Because experimental studies cannot sample this growth velocity
452 regime, we must leverage Earth's natural laboratory to estimate the salinity of ice formed in
453 these environments. We present a survey of the available published ice core data from Antarctica
454 and the Arctic, including samples of marine ice and sub-ice-shelf congelation ice (Fig. 4). We
455 provide characteristics of the environment in which the ice formed, including depth from the
456 surface as a proxy for temperature gradient (i.e., deeper ice implying a lower temperature
457 gradient) and estimates of growth velocity where available. We also include properties of the ice

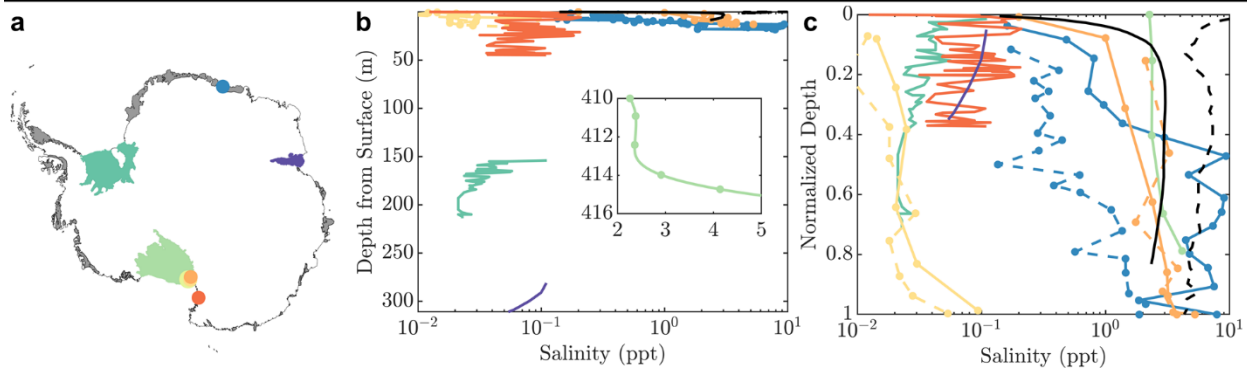
458 such as salinity and $\delta^{18}\text{O}$ where known, which can serve as a proxy for modification of the
 459 seawater by glacial meltwater (i.e., values close to 2‰ implying minimal modification). $\delta^{18}\text{O}$ is
 460 often used to determine the origin of the ice (i.e., marine or meteoric) when the salinity signal is
 461 ambiguous (Gow and Epstein 1972; Morgan 1972; Oerter *et al.* 1992). Estimates for the effective
 462 solute distribution coefficient were obtained by dividing the ice salinity by the salinity of
 463 seawater, assumed to be 35 ppt. Although it represents a relevant analog, we exclude the ice core
 464 from Lake Vostok because the mechanism of accretion remains debated, and the properties of
 465 the lake water are not well constrained (Souchez *et al.* 2000; Souchez *et al.* 2004; Lipenkov *et al.*
 466 2015). Table 3 presents the values of k_{eq} estimated from selected ice cores in Fig. 4. We discuss
 467 how these values are obtained in the following sections.

468 **TABLE 3.** Equilibrium distribution coefficients inferred from published samples of natural
 469 accreted ice from Earth. Values were derived using the minimum salinity observed in the core
 470 and an ocean salinity of 35 ppt. Where a trend (either increasing or decreasing) was absent in the
 471 salinity profile, the mean salinity was adopted instead. Only ice cores where melt water did not
 472 appear to contribute significantly to the salinity signal (i.e. $\delta^{18}\text{O} \approx 2$ in Fig. 4) were included. Ice
 473 type follows the same coding presented in Fig. 4 (SISC: Sub-Ice-Shelf Congelation Ice, M:
 474 Marine Ice).

k_{eq}	Ice Type	Sample	Source
6.7E-02	SISC	J-9 Ross Ice Shelf core	Zotikov <i>et al.</i> (1980)
7.4E-02	SISC	Columnar Ice from Hells Gate Ice Shelf	Souchez <i>et al.</i> (1991)
6.5E-02	SISC	Ice Island SP-6 core	Cherepanov (1964)
6.3E-02	SISC	Ice Island SP-4 core	Cherepanov (1964)
1.4E-03	M	AM01 Amery Ice Shelf core	Morgan (1972) in Eicken <i>et al.</i> (1994)
6.9E-04	M	B13 Filchner-Ronne Ice Shelf core	Moore <i>et al.</i> (1994)
1.7E-03	M	Nansen Ice Shelf core	Tison <i>et al.</i> (2001)

475

Location	Site Description	Name	Type	Depth from Surface (m)	Salinity (ppt)	$\delta^{18}O$ (ppt)	k	Growth Velocity (cm/s)	Source(s)
Amery Ice Shelf	Suture Zones	G1	M	270 – 315	0.05 – 0.1	0 – 2	10^{-3}	1×10^{-6}	Morgan (1972)
		AM01	M	276 – 376	0.03 – 0.56	2	$10^{-4} - 10^{-3}$	$\sim 10^{-6}$	Craven et al. (2004, 2009)
Roi Baudouin Ice Shelf	Rift Exposed at Surface	D	M	10 – 20	0.3 – 9	2	$10^{-2} - 10^{-1}$	-	Pattyn et al. (2012)
		E	M	0 – 15	0.3 – 2	2	$10^{-3} - 10^{-2}$	-	
Filchner-Ronne Ice Shelf	Thin Region beyond Henry Ice Rise	B13	M	152.8 – 215	0.02 – 0.1	2	$10^{-4} - 10^{-3}$	4×10^{-6}	Oerter et al. (1992) Eicken et al. (1994) Moore et al. (1994)
Ross Ice Shelf	Region of Heat Loss to the Ice Shelf	J-9	SISC	410 – 416	2 – 4	-	$10^{-3} - 10^{-2}$	$\sim 10^{-8}$	Zotikov et al. (1980)
McMurdo Ice Shelf	Exposed at Surface near Minna Bluff	Site 3	M	0 – 5	0.115	2.3	10^{-3}	-	Fitzsimons et al. (2012)
		C5	M	0 – 2.65	0.26 ± 0.11	1.63 ± 0.24	10^{-3}	-	Koch et al. (2015)
		C9	M	0 – 3.04	0.20 ± 0.15	1.64 ± 0.43	10^{-3}	-	
		C15	M	0 – 9.44	0.29 ± 0.18	0.47 ± 0.48	10^{-3}	-	
Dailey Islands	Exposed at Ice Shelf Surface	No. 1	M	0 – 6.74	0.01 – 0.09	-	$10^{-4} - 10^{-3}$	-	Gow et al. (1965)
		No. 2	M	0 – 15.25	0.01 – 0.05	-	$10^{-4} - 10^{-3}$	-	
Koettlitz Glacier Tongue	Exposed at Surface of Glacier Tongue	1	SISC	0 – 12.8	0.2 – 3.76	2.51 – 1.61	$10^{-3} - 10^{-1}$	-	Gow and Epstein (1972)
		3		0 – 13	2.19 – 5.26	1.76 – 1.85	$10^{-2} - 10^{-1}$	-	
Nansen Ice Shelf	Exposed in Rift at Ice Shelf Surface	NIS	M	0 – 45	0.005 – 0.19	1.80 – 2.37	$10^{-4} - 10^{-3}$	2×10^{-6}	Khazendar et al. (2001) Tison et al. (2001) Khazendar et al. (2003)
Hells Gate Ice Shelf	Exposed at Ice Shelf Surface	Granular	M	0 – 1.5	0.016 – 0.081	2 – 3.5	$10^{-4} - 10^{-3}$	-	3×10^{-7} Souchez et al. (1991)
		Columnar	SISC	0 – 1.5	1.6 – 2.6	1 – 2	10^{-2}	-	
		Platelet	M	0 – 1.5	0.24 – 0.49	2 – 3.5	$10^{-3} - 10^{-2}$	-	
Arctic	“Ice Island”	SP-6	SISC	0 – 9	0 – 3	-	10^{-2}	-	Cherepanov (1964)
	Sea Ice	9a	CS	0 – 1.5	4 – 7.5	-	10^{-1}	$\sim 10^{-5}$	Nakawo and Sinha (1981)



476

477 **FIG. 4.** A summary of properties and characteristics of terrestrial accreted ice from published
 478 ice core data. The first two columns specify the location where the ice core was collected and a

479 description of the sample site. The sites are color and texture coded by ice shelf and presented in
480 the map of Antarctica in (a). Where multiple cores were collected from a single location, the
481 second core is represented as dashed. The third column provides the name of the ice core as
482 referenced in the sources in the rightmost column. The type of accreted ice is specified in the
483 fourth column according to the following codes: M (Marine Ice), SISC (Sub-Ice-Shelf
484 Congelation Ice), CS (Congelation Sea Ice). The plots representing the (b) absolute and (c)
485 depth-normalized salinity profiles follow the same color and texture coding represented in the
486 table and map.

487 4.2.1. Sub-Ice-Shelf Congelation Ice

488 Samples of congelation ice formed in low temperature gradient environments are limited (Fig.
489 4). Unlike sea ice, where growth velocities can be estimated by periodic measurements over the
490 growth season (Nakawo and Sinha 1981), estimates of growth velocity for congelation ice
491 beneath ice shelves are obtained using models. Certain ice cores collected from ice shelves in
492 Antarctica (Ross Ice Shelf, Koettlitz Glacier Tongue, Hells Gate Ice Shelf) were observed to
493 have the columnar texture indicative of congelation ice (Gow and Epstein 1972; Zotikov *et al.*
494 1980; Souchez *et al.* 1991). Published estimates of the growth velocities associated with accreted
495 ice found beneath ice shelves (Fig. 4) are well within the asymptotic growth velocity regime of
496 the models in Fig. 3. Because of its extensive thickness, the sea ice island SP-6 likely approaches
497 temperature gradients within this regime and is thus also classified as sub-ice-shelf congelation
498 ice (Fig. 4). The salinity of accreted ice at these low temperature gradients can thus be used to
499 estimate k_{eq} for congelation ice (Table 3).

500 The bottom 2 cm of the Ross Ice Shelf core was described to have a “waffle-like” texture (Fig.
501 2), consistent with an actively growing congelation ice layer (Zotikov *et al.* 1980), often referred
502 to as a “skeletal layer” (Buffo *et al.* 2020). The salinity profile reveals a transition at
503 approximately 2 m above the ice-ocean interface from constant to monotonically increasing with
504 depth (Fig. 4b). In sea ice, an increase in salinity with depth near the base is recognized to be a
505 feature of growing sea ice (Eicken 1992). The increasing salinity observed near the base of the
506 Ross Ice Shelf core and the description of the basal texture suggest the bottom 2 m of the Ross
507 Ice Shelf core is in a state of active desalination. However, the constant salinity observed above
508 this transition can be considered the stable salinity, attained at growth rates within the asymptotic
509 regime (Fig. 3, 4), and can thus be used to obtain an estimate of k_{eq} (Table 3). The salinity
510 profiles associated with the Koettlitz Glacier Tongue ice cores do not appear to have achieved a
511 stable salinity, particularly the ice sampled from Hole 3 (Fig. 4c). This interpretation is supported
512 by samples of seawater obtained from the bottom of Hole 3, which was found to be enriched in
513 salt, suggesting the ice in this location is also actively desalinating (Gow and Epstein 1972).
514 Additionally, the $\delta^{18}\text{O}$ signal shows slight modification of the ice source water by glacial
515 meltwater. These observations suggest that the Koettlitz Glacier Tongue ice cores may not be
516 representative of an equilibrium state of salt partitioning, although the salinity profile of Hole 1
517 suggests a stable salinity could fall between 2 and 3 ppt which is in-family with the Ross Ice
518 Shelf core. A salinity profile is not available for the Hells Gate Ice Shelf columnar ice (Souchez

519 *et al.* 1991); however, the $\delta^{18}\text{O}$ signal presents with some evidence of modification by glacial
520 meltwater. Therefore, we adopt the maximum observed salinity to estimate a value for k_{eq} . The
521 salinity profile associated with Ice Island SP-6 drops off sharply near the ice-atmosphere
522 interface (Fig. 4c) which is indicative of post-genetic brine redistribution (Eicken 1992). As
523 such, for SP-6, we adopt the mean salinity to estimate k_{eq} assuming salt was redistributed in the
524 ice column but not removed (Cherepanov 1964). An ice core from Ice Island SP-4 was
525 referenced in Cherepanov (1964), although a salinity profile was not provided. We similarly use
526 the mean salinity specified for the SP-4 core to estimate k_{eq} . The equilibrium distribution
527 coefficients derived from these congelation cores are similar to one another and on the order of
528 10^{-2} (Table 3). Of the sub-ice-shelf congelation cores considered here, the salinity profile
529 associated with the Ross Ice Shelf core shows the least evidence of post-genetic desalination or
530 brine redistribution. The stable salinity of this ice core is representative of the effective
531 equilibrium solute distribution coefficient for natural congelation ice, $k_{eq} = 6.7 \times 10^{-2}$, which
532 is the same value inferred for the upper bound of the SP-6 core (Table 3). Notably, this value is
533 similar to the critical porosity of 5% for sea ice discussed in the previous section and is
534 consistent with the upper bound of 0.07 provided by Petrich and Eicken (2017). The observation
535 that the critical porosity appears to govern the bulk salinity of congelation ice even at low
536 temperature gradients (i.e., growth velocities $\sim 10^{-8}$ cm/s) lends credence to its potential for
537 governing the stable salinity of an ice shell formed through directional freezing.

538 4.2.2. Marine Ice

539 The distribution coefficients associated with marine ice can be lower than the equilibrium
540 distribution coefficients for congelation ice by up to two orders of magnitude (Table 3 and Fig.
541 4), generally falling between 10^{-4} and 10^{-3} (bulk salinities between 10^{-2} and 10^{-1} ppt). The
542 salinity profiles associated with marine ice (Fig. 4b,c) generally appear to depict a decrease with
543 distance from the meteoric-marine interface within the impermeable portion of the ice core and
544 an increase from the permeable-impermeable boundary to the ice-ocean interface. Note that
545 many of the profiles depicted in Fig. 4 do not extend to the permeable layer, so we must rely on
546 descriptions of the drilling and isolated samples reported in the published works to infer its
547 properties.

548
549 The salinity profiles of the Roi Baudouin Ice Shelf cores are anomalously high relative to those
550 of other marine ice cores (Fig. 4b,c) and approach values comparable to that of sea ice. Recent
551 consolidation was proposed as an explanation for the high salinity of the Roi Baudouin cores
552 (Pattyn *et al.* 2012), implying that young marine ice may initially present with salinities
553 commensurate with sea ice but will gradually desalinate and approach a steady state over time
554 due to increased accumulation and consolidation. This interpretation is supported by their
555 salinity profiles, which depict a stable salinity similar to that of the marine ice at McMurdo Ice
556 Shelf that transitions to an increasing salinity with depth (Fig. 4c). An alternative explanation is
557 that the Roi Baudouin marine ice formed in a high temperature gradient environment and is
558 analogous to platelet ice. However, the site is not unlike the rift at Nansen Ice Shelf where the
559 salinity of the marine ice there was found to be in-family with other marine samples (Khazendar

560 *et al.* 2001; Tison *et al.* 2001). The rift at Nansen Ice Shelf is located in an area with strong
561 katabatic winds, which could result in the ablation of the marine ice which originally infilled the
562 rift (Khazendar *et al.* 2001). This suggests the marine ice exposed at the surface may have
563 formed at a lower depth, much like at Hells Gate Ice Shelf where katabatic winds expose basal
564 marine ice at the surface near the ice shelf terminus (Souchez *et al.* 1991). This suggests marine
565 ice at Nansen ice shelf may have initially shared characteristics with that of Roi Baudouin but
566 became more homogenous and consolidated over time.

567
568 The age of the marine ice appears to be a more dominant factor in governing the bulk salinity
569 than the temperature gradient, supporting the idea that the consolidation mechanism is a
570 compaction and not congelation process. This is evident from the plots in Fig. 4c which
571 demonstrate that increased depth does not correlate to decreased salinity. Although the Dailey
572 Island cores correspond to the lowest salinity marine ice samples (Fig. 4c), because $\delta^{18}\text{O}$ was not
573 measured, the role of glacial meltwater in reducing the salinity cannot be discounted. The
574 salinities of the Nansen Ice Shelf core, Filchner-Ronne Ice Shelf core, and the Amery Ice Shelf
575 core are approximately equal although they were sampled from depths that differed by over 100
576 m from each other. The profiles associated with the Amery Ice Shelf and Nansen Ice Shelf cores
577 suggest the salinity could continue decreasing beyond the region sampled. As such, the
578 equilibrium distribution coefficients derived from these cores may be overestimates (Table 3).
579 The Filchner-Ronne Ice Shelf core, on the other hand, shows evidence of achieving a stable
580 salinity near the base of the core. We thus adopt $k_{eq} = 6.9 \times 10^{-4}$ as the effective equilibrium
581 solute distribution coefficient for low temperature gradient frazil ice, which corresponds to the
582 stable salinity of the consolidated layer estimated using the salinity at the base of the Filchner-
583 Ronne Ice Shelf core (Fig. 4).

584

585 5. Accretion beneath the Ice Shells of Ocean Worlds

586 Although there have been no direct observations of the interior of the ice shells of ocean worlds,
587 features observed at the surfaces or inferred about the ice shell topography have led to the
588 development of hypotheses for processes that either directly appeal to the accretion of ice at the
589 ice-ocean interface or are consistent with conditions that promote it (e.g., Soderlund *et al.* 2020).
590 These features are scars of processes which modify bulk ice shell properties and serve as a record
591 of heterogeneities introduced into the native shell.

592 5.1. Bulk Salinity of a Congelation Ice Shell

593 We estimate the bulk salinity of the ice shell as the product of congelation ice growth at the ice-
594 ocean interface using a 1D solidification model known as the Stefan problem, where heat is
595 conducted from the interface through the overlying ice. This model has been previously applied
596 to Europa's ice shell (see Buffo *et al.* (2021b) and Quick and Marsh (2015)); however, we
597 specifically adopt the form published in Lior (1996). The analytical solution to this problem
598 represents the temperature in the ice, T , as a function of position, x , and time, t , and is given by

$$T(x, t) = T_s + (T_f - T_s) \frac{\operatorname{erf}\left(\frac{x}{2\sqrt{\alpha t}}\right)}{\operatorname{erf}(\lambda')} \quad (1)$$

599

600 where T_s is the surface temperature, T_f is the freezing temperature, α is the thermal diffusivity of
 601 the ice, and λ' is the solution to the equation

$$\lambda' e^{\lambda'^2} \operatorname{erf}(\lambda') = \frac{N_{Ste}}{\sqrt{\pi}} \quad (2)$$

602

603 where N_{Ste} is the Stefan Number, defined as

$$N_{Ste} = \frac{c_p(T_s - T_f)}{L} \quad (3)$$

604

605 where c_p is the specific heat capacity of ice and L is the latent heat of fusion. The position of the
 606 ice-water interface as a function of time can be expressed in terms of these variables as

$$X(t) = 2\lambda'\sqrt{\alpha t} \quad (4)$$

607

608 and the velocity of the ice-water interface is

$$v = \dot{X}(t) = \lambda' \sqrt{\frac{\alpha}{t}} \quad (5)$$

609

610 which corresponds to the time derivative of Eq. 4. We use Eq. 5 to estimate ice shell growth rate
 611 as a function of the ice-water interface position, represented by ice thickness (Fig. 5). We assume
 612 the ocean is at the melting temperature of 270 K and that the thermophysical properties of the ice
 613 shell are represented by pure ice at this same temperature at 1 atm (Feistel and Wagner 2006).
 614 We evaluate four cases, assuming upper boundary conditions of 50 K, 100 K, 200 K, and 250 K
 615 to approximate surface temperatures expected at icy ocean worlds. 50 K represents a lower
 616 bound surface temperature for both Europa and Enceladus, 100 K represents the mean annual
 617 surface temperature of Europa's ice shell (Ojakangas and Stevenson 1989; Ashkenazy 2019),
 618 200 K represents the maximum temperature near the tiger stripes of Enceladus (Spencer *et al.*
 619 2018), and 250 K is intended to represent a terrestrial boundary condition. Higher surface
 620 temperatures result in lower growth rates for a given ice shell thickness. Using this model, we
 621 can estimate an upper bound on ice shell growth rate and thus estimate the maximum salinity of
 622 the bulk ice shell.

623 Instead of explicitly modeling salt rejection, like Buffo *et al.* (2020) and Buffo *et al.* (2021a), we
 624 represent the incorporation of salt as a function of growth velocity using a model for $k(v)$,
 625 adapted from Petrich *et al.* (2011). We prescribe a critical porosity equal to the effective
 626 equilibrium distribution coefficient for congelation ice $\phi_c = k_{eq}$, as opposed to $\phi_c = 0.05$ which
 627 is used in the model of Petrich *et al.* (2011), and force the model to approach this value at low

628 growth velocities. This yields an expression for the effective solute distribution coefficient given
 629 by

$$k(v) = k_{eq} \left(1 + \frac{k_{eq}}{2} \frac{v}{\gamma_s w_0} \left[-1 + \sqrt{1 + \frac{4(1 - k_{eq}) \gamma_s w_0}{k_{eq}^2 v}} \right] \right) \quad (6)$$

630

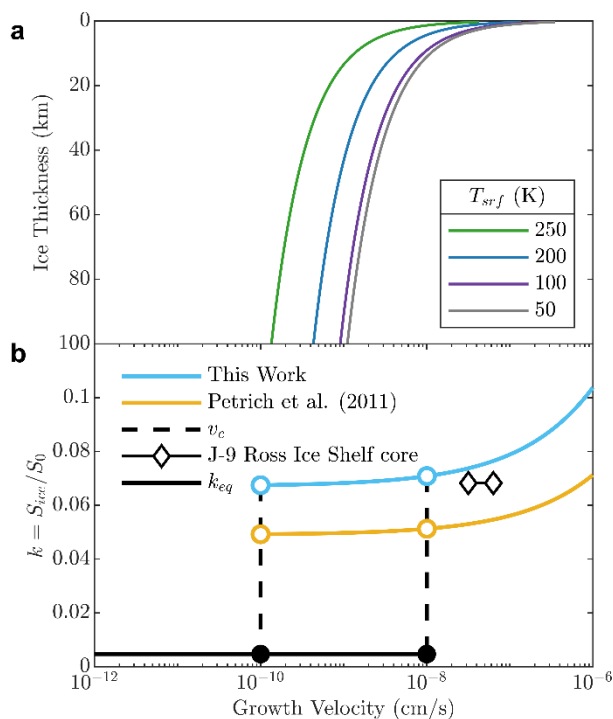
631 where k_{eq} represents the effective equilibrium solute distribution coefficient for congelation ice,
 632 v is the ice growth velocity, and $\gamma_s w_0$ represents a scaling parameter related to the interstitial
 633 brine velocity (Petrich and Eicken 2017). Note that our version includes an additional factor of 2
 634 that was excluded from a term in the radicand in the published versions of the original model
 635 (Petrich *et al.* 2011; Petrich and Eicken 2017). We fit Eq. 6 to the data of Nakawo and Sinha
 636 (1981) to obtain $\gamma_s w_0 = 3 \times 10^{-8}$ m/s which is similar to the value of $\gamma_s w_0 = 4.5 \times 10^{-8}$ m/s
 637 obtained by Petrich *et al.* (2011). Both our model and the original model are shown alongside the
 638 data of Nakawo and Sinha (1981) in Fig. 3. We estimate the bulk salinity of the ice shell using
 639 Eq. 6 and the growth velocities obtained from the 1D freezing model (Eq. 5). We find that the
 640 growth velocity transitions to the ice shelf regime (Fig. 3) below ~ 100 m depth for all surface
 641 temperatures considered. This is similar to the results of Buffo *et al.* (2020) which found the
 642 salinity profile approaches an asymptotic value below ~ 300 m. This supports the conclusion that
 643 the bulk salinity for a large fraction of the ice shell will correspond to a value approaching the
 644 effective equilibrium solute distribution coefficient. Note that the lower limit bulk ice shell
 645 salinity predicted by Buffo *et al.* (2020) corresponds to an effective equilibrium solute
 646 distribution coefficient governed by the apparent critical porosity in congelation ice (~ 0.05). We
 647 instead adopt an effective equilibrium solute distribution coefficient of $k_{eq} = 6.7 \times 10^{-2}$,
 648 derived from the Ross Ice Shelf core in Section 4.2.1 to represent the bulk salinity of a
 649 congelation ice shell.

650 Although the critical porosity appears to be a significant factor governing the effective
 651 equilibrium solute distribution coefficient in natural congelation ice, as the growth velocity
 652 approaches zero, the ice-water interface geometry should become planar and as a result will be
 653 incapable of entrapping brine (Eicken 1998). A planar interface is generally stable for lake ice on
 654 Earth because of the relative purity of the water ($\lesssim 1$ ppt); however, the same phenomenon can
 655 occur if the growth velocity falls below a critical growth velocity for a higher salinity water
 656 (Wettlaufer 1992; Maus 2007). The development of a stable planar interface under the
 657 appropriate growth conditions is a phenomenon that has been studied in both nature and
 658 laboratory experiments for decades (Weeks and Lofgren 1967; Grothe *et al.* 2014). In
 659 experiments the transition from a cellular to planar interface coincides with a drastic change in
 660 appearance (cloudy to clear) and a reduction in effective solute distribution coefficient that can
 661 exceed an order of magnitude (Weeks and Lofgren 1967; Osterkamp and Weber 1970; Kvajić
 662 and Brajović 1971; Maus 2006). This suggests the potential existence of a congelation ice shell
 663 where the bulk salinity is not governed by the critical porosity.

664 Although the existence of a critical growth velocity is not controversial, the magnitude of the
 665 critical growth velocity for a solution of a given salinity is challenging to constrain.
 666 Morphological stability theory (MST), originally proposed by Mullins and Sekerka (1964), has
 667 been leveraged by a number of authors to investigate the development of a cellular interface in

668 the freezing of saltwater systems (Wettlaufer 1992; Maus 2007). The theory has been augmented
669 through the years (Coriell *et al.* 1985; Sekerka *et al.* 2015) and is still an active area of research
670 (Maus 2020). The theory predicts the existence of a critical growth velocity below which a
671 planar ice-water interface should be stable for any wavelength perturbation. The magnitude of
672 this critical growth velocity is poorly constrained by theory and is highly sensitive to parameters
673 including the solution concentration (i.e., salinity), the interfacial solute distribution coefficient
674 (S_{ice}/S_{int}), and the temperature gradient in the liquid (Terwilliger and Dizio 1970; Wettlaufer
675 1992; Maus 2006; Maus 2020). To illustrate the onset of this transition during the thickening of
676 an ice shell (Fig. 5), we adopt the values obtained by Wettlaufer (1992) from a linear stability
677 analysis applied to the interface morphology of a sodium chloride system for a solution
678 concentration approximately equal to Earth's ocean (~35 ppt). The critical growth velocity of
679 $v_c \approx 10^{-8}$ cm/s assumes an interfacial solute distribution coefficient of 0.3, whereas $v_c \approx 10^{-10}$
680 cm/s assumes an interfacial solute distribution coefficient of 0.003. Their results demonstrate that
681 the more efficient the ice is at rejecting the solute, the lower the critical velocity for the onset of
682 interface instability for a given solution concentration. The upper estimate for critical growth
683 velocity is reached for an ice shell thickness less than ~10 km for all surface temperatures
684 considered (Fig. 5). Again, note that we adopt the values in Fig. 5 for illustration purposes only
685 and the true value could be orders of magnitude lower.

686
687
688
689
690



691
 692 **FIG. 5. (a)** Ice shell thickness vs. growth velocity and **(b)** effective solute distribution coefficient
 693 vs. of growth velocity. The effective solute distribution coefficient curves are taken from Fig. 3.
 694 The dashed line represents an illustration of the transition from a cellular interface to a planar
 695 interface at a critical growth velocity, v_c , represented by two possible values. The solid line
 696 depicts the equilibrium solute distribution coefficient from Gross *et al.* (1977). The diamond
 697 markers represent the bounds of growth velocity estimated by Zotikov *et al.* (1980) for the J-9
 698 Ross Ice Shelf core.

699 Below the critical velocity, we assume a planar-ice water interface remains stable and that the
 700 bulk salinity of the ice shell will be governed by the equilibrium distribution coefficient (note the
 701 absence of “effective”) for congelation ice, where impurities are retained predominantly within
 702 the ice lattice (i.e., not incorporated interstitially as brine). However, soluble salts can be
 703 accommodated in the ice lattice only up to a certain concentration referred to as the solubility
 704 limit. From both natural and artificial samples, the solubility limit for chloride in ice has been
 705 inferred to be $\sim 300 \mu\text{M}$ (Seidensticker 1972; Gross *et al.* 1977; Moore *et al.* 1994), although in
 706 the presence of ammonium the solubility limit increases (Gross *et al.* 1977). There is some
 707 evidence that the solubility limit may be higher in ice that has undergone recrystallization
 708 (Moore *et al.* 1994), suggesting marine ice may be able to accommodate more chloride than sub-
 709 ice shelf congelation ice. The chloride distribution coefficients obtained by Gross *et al.* (1977)
 710 represent salt entrainment through incorporation of impurities in the ice lattice and serve as the
 711 lower bound of equilibrium distribution coefficients for congelation ice. Their values are similar
 712 to earlier works that estimated equilibrium distribution coefficients on the order of 10^{-3} for
 713 dilute ($\sim 2 \times 10^{-4}$ M) chloride solutions (Osterkamp and Weber 1970). For solution
 714 concentrations where chloride could be entirely accommodated within the ice lattice ($\lesssim 10^{-1}$ M)
 715 and did not occupy interstitial sites, the average equilibrium distribution coefficient was

716 determined to be $k_{eq} = 2.7 \times 10^{-3}$ (Gross *et al.* 1977). Note that this distribution coefficient
717 applies to chloride and not the associated cation pair, which was found to be significantly less
718 soluble (Gross *et al.* 1977). In the presence of ammonium, the equilibrium distribution
719 coefficient increased to $k_{eq} = 1.4 \times 10^{-2}$ (Gross *et al.* 1977). For more concentrated solutions,
720 the solubility limit was exceeded upon crystallization, forcing residual impurities to be
721 accommodated interstitially along grain boundaries. In this case the distribution coefficient
722 increased to $k_{eq} = 4.7 \times 10^{-3}$ (Gross *et al.* 1977; Tison *et al.* 2001). Although the distribution
723 coefficient almost doubled at this transition, it was independent of the solution concentration
724 both below and above this transition. It is unclear whether a solution composed entirely of
725 insoluble salts, such as magnesium sulfate, would be accommodated as efficiently because it
726 would be limited to interstitial sites. It is also possible that because of its inability to be
727 accommodated in the lattice, a solution dominant in lattice insoluble salts may promote interface
728 breakdown and enhance interstitial entrapment.

729 These models imply that the native bulk salinity of a congelation ice shell should be <10% of the
730 ocean salinity, where sub-ice-shelf congelation ice cores imply a bulk salinity between 6% and
731 7%. There are two cases where we might expect a higher salinity layer to be present near the ice
732 shelf surface: (i) catastrophic melting and subsequent refreezing of an ice shell, although this
733 would likely only extend to ~100 m depth, and (ii) rapid refreezing of intrusive features, if they
734 extend far enough into the cold ice shell interior (Buffo *et al.* 2020). If the ice shell growth
735 velocity is sufficiently slow, such that a planar interface remains stable as the ice shell thickens,
736 the ice shell salinity reduces to <1% of the ocean salinity. For a planar interface at near-
737 equilibrium conditions, the salts entrained are dominantly lattice soluble salts, such as chloride.
738 The experiments of Gross *et al.* (1977) suggests the ice chlorinity will be 0.27% of the ocean
739 chlorinity. In the case that the chlorides cannot be entirely accommodated within the lattice, the
740 ice shell chlorinity will be 0.47% of the ocean chlorinity and permit some interstitial
741 incorporation of impurities. Diagenetic processes can operate to alter the bulk ice shell salinity
742 post-accretion. Flushing of interstitial impurities by meltwater could locally reduce the ice shell
743 salinity, whereas refreezing of meltwater could locally enhance the ice shell salinity. In the ice
744 shells of ocean worlds, meltwater may be generated through tidal heating (Sotin *et al.* 2002),
745 through frictional heating caused by tectonic activity (Gaidos and Nimmo 2000; Nimmo and
746 Gaidos 2002), or by convective currents (Kalousová *et al.* 2014). Whether this melt can drain
747 through the ice shell is critically dependent on the ice shell permeability (Kalousová *et al.* 2014;
748 Hesse *et al.* 2020). If interstitial impurities are removed due to flushing or drainage, the bulk
749 salinity would be governed by concentration of impurities accommodated in the ice lattice. For
750 ice saturated with chloride, this would imply an ice shell chlorinity of ~10 mg/kg which is on the
751 order of ice shell salinity predicted by Steinbrügge *et al.* (2020).

752 Fluctuations in ice shell growth rates have the potential to generate vertical and regional
753 heterogeneities in ice shell salinity. However, predicted growth rates suggest fluctuations are
754 likely to fall within the low growth velocity regime (Table 2, Figure 3), where the effective
755 solute distribution coefficient is relatively insensitive to changes in growth velocity. Peddinti and
756 McNamara (2019) predict an increase in growth rate from 5.67 km/Myr to 8.22 km/Myr
757 associated with the merging of convective cells within Europa's ice shell, which translates to

758 growth velocities of 1.8×10^{-8} to 2.6×10^{-8} cm/s. Growth rate estimates obtained by other
759 authors are typically on the order of 10^{-9} or 10^{-8} cm/s (Table 2). Comparing the lowest
760 estimate of freezing rate for Europa's ice shell in Table 2 (~ 1.5 km/Myr) to the age of the surface
761 (~ 100 Ma) would imply an ice shell thickness of ~ 150 km (Bierhaus *et al.* 2009). Because
762 Europa's ice shell thickness is thought to be an order of magnitude thinner, this suggests (i) the ice
763 shell has reached a near-equilibrium thickness, (ii) the ice shell is in a state of thermodynamic
764 disequilibrium where melting and re-freezing are occurring continuously, as suggested by Green
765 *et al.* (2021), or (iii) the estimated freezing rates are potentially an order of magnitude higher
766 than reality. At Enceladus, observed topographic anomalies are thought to be maintained by
767 melting/freezing less than a few mm/yr (Čadek *et al.* 2019; Kang *et al.* 2021), which translates to
768 growth velocities on the order of 10^{-9} cm/s. These growth velocities are comparable to the upper
769 estimate for critical growth velocity at which an ice-water interface becomes planar for a
770 terrestrial ocean (Wettlaufer 1992). If transitions in growth velocity are such that the ice-water
771 interface stability is affected, this could result in a salinity contrast of up to an order of
772 magnitude associated with this event (Fig. 5). A similar magnitude salinity contrast could be
773 generated by the local and regional accretion of marine ice beneath congelation ice.

774

775 5.2. Local and Regional Accretion of Frazil Ice

776 The ice-ocean interfaces of icy ocean worlds represent dynamic environments characterized by
777 gradients in ice thickness on both regional and local scales (Nimmo *et al.* 2007; Nimmo and Bills
778 2010; Čadek *et al.* 2019; Hemingway and Mittal 2019; Soderlund *et al.* 2020).

779 Rifts and basal features, such as crevasses and troughs, represent favorable locations for the
780 formation and accretion of frazil ice in an ice shell. A number of processes have been
781 demonstrated to generate stresses sufficient to cause fracturing in the ice shell including impacts
782 (Craft and Roberts ; Turtle and Pierazzo 2001), pressurization due to cooling and thickening
783 (Nimmo 2004b; Manga and Wang 2007; Johnston and Montési 2017; Hemingway *et al.* 2020),
784 tidal forcing/nonsynchronous rotation (Helfenstein and Parmentier 1985; Geissler *et al.* 1998;
785 Greenberg *et al.* 1998; Hoppa 1999; Lee *et al.* 2005; Hurford *et al.* 2007; Rhoden *et al.* 2012;
786 Patthoff *et al.* 2019), and true polar wander (Schenk *et al.* 2008; Rhoden *et al.* 2011; Tajeddine *et al.* 2017).

788 The fracturing of an ice shell has important implications for surface-ice-ocean exchange and as
789 such has been studied extensively. Early work by Crawford and Stevenson (1988) examined both
790 surface and basal fractures as resurfacing mechanisms for Europa's ice shell. They found that
791 direct conduits extending from the surface through an ice shell were unlikely due to the need for
792 high stresses applied rapidly which cannot be supplied by any process thought to be operating at
793 Europa. Basal fractures were also shown to be incapable of extending to the surface; however,
794 they extended over an order of magnitude farther than surface fractures. Although basal ice is
795 ductile, Crawford and Stevenson (1988) argue that crack initiation and propagation is possible if
796 the ice is strained sufficiently rapidly compared to the Maxwell time. This condition is possibly
797 satisfied by the eccentricity tides which are $\sim 10^5$ s and comparable to the Maxwell time of $\sim 10^4$

798 s (Crawford and Stevenson 1988). The model of Lee *et al.* (2005) showed that surface fractures
799 could penetrate the entire brittle part of the ice shell, in the case where a brittle and ductile layer
800 are mechanically decoupled. They did not study basal fractures, citing that they were less likely
801 to occur than surface fractures based on the increase in ice strength with depth, due to pore
802 closure, and their interpretation of the results of Crawford and Stevenson (1988). Rudolph and
803 Manga (2009) show that in the presence of a relaxed basal layer, fractures on Europa cannot
804 penetrate the ice shell for thicknesses greater than a few kilometers. Because the gravitational
805 acceleration at Enceladus is a fraction of that at Europa, fractures could penetrate the ice shell for
806 thicknesses up to tens of kilometers (Rudolph and Manga 2009). The ice shell thickness where
807 the tiger stripes are located is thought to be less than 10 km (Hemingway *et al.* 2020), supporting
808 the interpretation that these features are fractures connecting the ice shell surface to a subsurface
809 ocean (Postberg *et al.* 2011; Spencer *et al.* 2018). The ice collapse model of Walker and Schmidt
810 (2015) suggests basal fractures could form above a subsurface water pocket; however, this
811 mechanism would not necessarily translate to the formation of basal fractures at an ice-ocean
812 interface. Hemingway *et al.* (2020) argue that a surface fracture could penetrate a ductile ice
813 layer in an ice shell, so long as it is not too thick, because the layer will behave elastically on
814 timescales relevant to fracture propagation. Walker *et al.* (2021) show that tensile fractures
815 initiating from the base of an ice shell can propagate further into the interior than surface
816 fractures. Furthermore, they showed that connection between the surface and ice-ocean interface
817 can be achieved if basal tensile fractures connect to the surface through shear failure.

818 Broadly these works suggest basal fractures extending into the ice shell interior are possible—if
819 the basal ice is subject to a sufficiently high strain rate—and that rifts extending through the
820 entirety of an ice shell are unlikely for Europa but possible under specific conditions. Still, many
821 authors attribute surface features at Europa such as domes, pits, and lenticulae to the presence of
822 sills within the ice shell and implicate vertical fractures extending from the ice-ocean interface in
823 their formation (e.g., Michaut and Manga 2014; Craft *et al.* 2016). Furthermore, observations
824 and interpretations of putative plume activity at Europa (e.g., Sparks *et al.* 2017; Jia *et al.* 2018)
825 and Enceladus (e.g., Postberg *et al.* 2011) provide strong evidence that fractures in the ice shell
826 serve as a connection between the surface and some subsurface water reservoir. Where cracks
827 may penetrate the entirety of an ice shell, such as the tiger stripes at Enceladus, the resulting
828 plumes would likely include samples of relatively unfractionated ice formed from agglomerated
829 frazil crystals that nucleated within the turbulent, supercooled water column as the ocean water
830 was brought to the surface. Given the fast rate of ice formation, the salinity and compositional
831 signal likely experiences minimal fractionation, $k \approx 1$. Conversely, if the plume material were
832 sourced from a reservoir generated from the melt of native ice shell material and not the ocean,
833 our estimate of the effective equilibrium solute distribution coefficient for a congelation ice shell
834 ($k_{eq} = 6.7 \times 10^{-2}$) would predict a saturated ocean at Enceladus (20 ppt/0.067 ~ 300 ppt). This
835 estimate neglects the effect of brine concentration that may occur during freezing of a reservoir.
836 At Enceladus, plume material is thought to be sourced directly from a sub-ice ocean (Spencer *et al.*
837 *et al.* 2018); however, the origin of plumes at Europa is more ambiguous (Sparks *et al.* 2017).

838 Ice shell thickness variations on regional scales have been inferred from models and observations
839 of ocean worlds. Models of the ice shell thickness of Enceladus based on observations of the
840 shape (Tajeddine *et al.* 2017) and gravity (Iess *et al.* 2014) by *Cassini* suggest the presence of
841 lateral variations in the ice shell thickness (Čadek *et al.* 2019). Limb profiles of Europa suggest

842 either a thin ice shell (<35 km) with lateral thickness variations below the detection threshold or
843 a thicker shell in which lateral flow or convection promote a uniform ice shell thickness (Nimmo
844 *et al.* 2007). Although the ice shell thickness of Europa is more poorly constrained than
845 Enceladus (Billings and Kattenhorn 2005; Howell 2021), multiple models have demonstrated
846 variations in surface temperature and basal heat flux could promote lateral thickness gradients
847 (e.g., Soderlund *et al.* 2013; Ashkenazy *et al.* 2018; Āadek *et al.* 2019; Soderlund 2019). These
848 lateral thickness gradients could plausibly occur in any icy ocean world with large surface
849 temperature gradients in latitude and/or heterogeneous tidal heating. Because these lateral
850 thickness gradients are unstable (both from a mechanical and thermodynamic perspective),
851 mechanisms will operate to homogenize the ice shell thickness.

852 Two mechanisms have been proposed for the homogenization of ice shell thickness: (i) the
853 pressure gradient induced by the variable ice thickness will drive basal ice flow from thicker to
854 thinner regions of the ice shell (e.g., Ojakangas and Stevenson 1989; Nimmo 2004a; Nimmo *et*
855 *al.* 2007; Ashkenazy *et al.* 2018) and (ii) an “ice pump”, described by Lewis and Perkin (1986),
856 will operate to melt ice where the ice shell is thick and accrete ice where the ice shell is thin
857 (e.g., Vance and Goodman 2009; Soderlund *et al.* 2013). Both properties likely play a role in
858 homogenizing ice shell thickness gradients, although environmental factors such as ocean
859 circulation and tidal velocity will determine which process dominates (Goodman 2018). The ice
860 flux resulting from viscous flow at the base of the ice shell has been estimated to range from
861 fractions of a millimeter to centimeters per year at Europa (Ashkenazy *et al.* 2018) and less than
862 a few millimeters per year at Enceladus (i.e., on the same timescales as melting) (Kamata and
863 Nimmo 2017), whereas marine ice accretion rates on Earth, driven by the “ice pump” are on the
864 order of meters per year (Craven *et al.* 2009). We thus focus our discussion on the “ice pump”
865 which could infill these features on shorter timescales than viscous flow. As the buoyant
866 meltwater is transported along the ice-ocean interface in the direction of decreasing ice thickness,
867 it will become supercooled due to the reduction in pressure and prime the generation of frazil ice.

868 For terrestrial ice shelves, the ice pump process is approximately adiabatic (Foldvik and Kvinge ;
869 Tison *et al.* 1998; Koch *et al.* 2015; Hoppmann *et al.* 2020). Neglecting heat transfer between
870 water masses is likely only a valid assumption over certain temporal and spatial scales, which
871 may be exceeded when applied to regional scale thickness gradients in the ice shells of ocean
872 worlds. Crevasses, troughs, and rifts, on the other hand, represent high gradient features that can
873 promote substantial supercooling through the operation of a highly localized ice pump. The
874 magnitude of potential supercooling will be governed by the feature’s vertical extent in the ice
875 shell, equivalent to the difference in the pressure melting temperature expected by a reduction in
876 overburden pressure (Fig. 1). These high gradient features also provide a means to shelter the
877 frazil from potentially strong sub-ice currents (Soderlund *et al.* 2020), allowing crystals to
878 accumulate and consolidate, forming marine ice. This process is analogous to the infilling of rifts
879 at the Nansen and Roi Baudouin Ice Shelves by marine ice (Fig. 4). The texture of the Nansen
880 Ice Shelf core was not columnar, suggesting no congelation growth had occurred within the rift
881 (Khazendar *et al.* 2001). This suggests the infilling of high gradient features in the ice shells of
882 ocean worlds would likely be dominated by frazil ice, as opposed to congelation ice, by nature of
883 both the localized ice pump and the relatively low temperature gradients expected near the base
884 of the ice shell. In this case, the salinity profile will likely decrease with depth within the
885 consolidated layer. At the permeable-impermeable boundary, the salinity may appear to level off

886 before increasing again as the brine volume fraction increases with depth (Fig. 4). It is possible
887 that if the fracture penetrated far enough into the ice shell such that the surrounding ice was
888 substantially colder, congelation ice could play more of a role as modeled in Buffo *et al.* (2020).

889

890 6. Implications of Accretion at the Ice-Ocean Interface

891 6.1. Geophysical Implications of Heterogeneous Accretion

892 The accretion of frazil ice within basal features in a congelation ice shell has significant
893 implications for processes governing surface-ice-ocean exchange. Frazil ice accretion serves as a
894 vehicle to deliver both sensible heat and latent heat into the ice shell interior. Sensible heat is
895 delivered through the introduction of warm ice (relative to the ice shell interior), as frazil infills
896 and consolidates within basal features. The relative warmth of marine ice within an ice shelf is
897 supported by borehole measurements from Amery Ice Shelf which show that the temperature
898 profile within the marine ice layer is nearly isothermal at a temperature close to the freezing
899 point of the underlying seawater (Craven *et al.* 2009). The gradual consolidation and interstitial
900 freezing of brine pockets further releases latent heat into the ice shell, serving as an additional
901 mechanism to thermally perturb the ice shell. Because of the timescales of tidal cycles on
902 Enceladus, it is unlikely a highly-consolidated marine ice would be able to form within the tiger
903 stripes; however, the formation and accumulation of frazil in the fissures could be capable of
904 modulating eruptions, a role previously attributed to turbulent dissipation alone (Kite and Rubin
905 2016).

906 Marine ice is more ductile than meteoric ice (Holland *et al.* 2009; Jansen *et al.* 2013; Kulesa *et al.*
907 *et al.* 2014; McGrath *et al.* 2014); however, it is still an open area of research whether this could be
908 an intrinsic material property or can be attributed to elevated temperatures alone (Dierckx and
909 Tison 2013; Craw 2020). The infilling of basal features by more ductile ice could affect the
910 mechanical properties of the ice shell. On Earth, marine ice accretion is thought to play an
911 important role in stabilizing ice shelves against collapse through the infilling of regions of
912 weakness (Holland *et al.* 2009; Khazendar *et al.* 2009; Kulesa *et al.* 2014) and could play a
913 similar role in ice shells. The observation that fractures propagating in ice shelves arrest when
914 encountering features infilled with marine ice (McGrath *et al.* 2014) could guide inferences of
915 subsurface properties of an ice shell using observations of the fractured surface terrain. The
916 accretion of marine ice within suture zones has been shown to channel shear deformation
917 enabling decoupling of adjacent units of ice flowing at different velocities (Jansen *et al.* 2013).
918 As such, accretion in pre-existing fractures could facilitate strike-slip and lateral displacement,
919 thought to be responsible for the linea observed on Europa's surface (Hoppa 1999; Hoppa *et al.*
920 2000; Prockter *et al.* 2000; Hammond 2020). Enhanced ductility within these features might also
921 favor heating over fracturing when subject to tidal deformation, potentially resulting in positive
922 feedback. The enhanced ductility would also increase the Rayleigh number (ratio of buoyancy to
923 diffusion), influencing convective vigor and modulating its responses to tidal forcing. This
924 suggests marine ice accretion could also play a role in transitioning between convective and
925 conductive regimes in an ice shell.

926 The marine ice infilling these features is not only warmer but could also be significantly purer
927 than the native ice shell material (see Table 3). As such marine ice is both thermally and
928 compositionally buoyant, which could further promote the formation of narrow diapirs thought
929 to be responsible for forming Europa's domes (Pappalardo and Barr 2004). Soderlund *et al.*
930 (2013) proposed that marine ice accretion on regional scales, modulated by thickness gradients
931 established by heterogeneous ocean-driven heating, could play a role in the formation of chaos
932 terrain through a similar mechanism (Schmidt *et al.* 2011).

933

934 6.2. Fractionation

935 To constrain the habitability of an ocean world, it is important to determine whether the
936 composition of the ice shell is representative of the underlying ocean. Knowledge of the
937 composition of the sub-ice ocean would help decipher whether the ocean is in an oxidizing or
938 reducing state (Zolotov 2008), which in turn would help guide future life-detection missions. In a
939 reducing ocean organisms might concentrate at the ice-ocean interface where surface oxidants
940 delivered to the ocean could drive metabolism-supporting redox gradients, whereas in an
941 oxidizing ocean organisms might concentrate at the sea floor where water-rock interactions
942 and/or hydrothermal activity could supply reductants (Vance *et al.* 2016; Russell *et al.* 2017).
943 Directly sampling the sub-ice ocean to constrain its composition is a significant engineering
944 challenge (Bryson *et al.* 2020). Studying the surface or near-surface composition, while still an
945 engineering challenge, represents a more feasible approach in pursuit of constraining the
946 composition and thus redox state of the sub-ice ocean (Hand 2017). The mode of salt
947 entrainment, whether salt is accommodated within the ice lattice or interstitially as brine pockets,
948 can influence the ice shell composition. A cellular interface would be more favorable for the
949 entrapment of brine pockets than a planar interface, resulting in a bulk ice composition more
950 representative of the underlying ocean in terms of the *relative* concentrations of major ionic
951 species. Because there are very few studies of the chemistry of low temperature gradient ice, we
952 include studies of sea ice to identify processes that can result in fractionation of an ice shell.

953 The composition of sea ice is generally assumed to be representative of seawater (Petrich and
954 Eicken 2017), although published studies of accreted ice chemistry suggest that some chemical
955 fractionation occurs in sea and marine ice (Table 4). There does not appear to be any evidence
956 that sulfate or calcium are consistently either enriched or depleted in sea ice, although potassium
957 appears to be depleted across all sea ice samples presented in Table 4. This is consistent with the
958 idea that the degree of fractionation should scale with ion diffusivity because potassium
959 represents the fastest diffusing ion and thus is more efficiently removed from the ice through
960 networks of brine channels (Maus *et al.* 2011). The consistent enrichment of magnesium
961 observed in sea ice (Table 4), cannot be attributed to known cryohydrate precipitation and is
962 likely related to its slow diffusivity relative to chloride (Granskog *et al.* 2004; Maus *et al.* 2011).
963 Although calcium and sulfate are also slow diffusing relative to chloride, these ions participate in
964 cryohydrate formation early-on in sea ice growth ($T > -8$ °C) which could further influence the
965 fractionation signal. Studies of fractionation in multi-year sea ice cores (Anderson and Jones
966 1985; Gjessing *et al.* 1993) and changes in fractionation with depth observed in young sea ice
967 cores (Maus *et al.* 2011) suggest that the fractionation signal may evolve as the ice thickens and

968 ages. The mixing model of Reeburgh and Springer-Young (1983) suggests that melt produced
 969 from warming as the ice ages removes ionic species conservatively; however, the sea ice samples
 970 of Gjessing *et al.* (1993) show strong sulfate depletion due to washout from melting snow. The
 971 enrichment observed in certain low salinity samples was interpreted to the result of refreezing of
 972 meltwater (Gjessing *et al.* 1993). Although mirabilite precipitation is often implicated in
 973 observed sulfate enrichment (Granskog *et al.* 2004), the results of Gjessing *et al.* (1993) and
 974 Maus *et al.* (2011) suggest sulfate enrichment could be due to the relatively low diffusivity of
 975 sulfate. Because chloride can be accommodated in the lattice, it can be preserved in the ice as
 976 other insoluble ions retained in interstitial brine are rejected (Moore *et al.* 1994). This
 977 phenomenon can be observed in samples of marine ice, where the degree of fractionation appears
 978 to increase and chloride becomes more enriched as brine volume fraction and salinity decreases
 979 (Moore *et al.* 1994). Snow ice similarly appears to retain chloride relative to other ions when
 980 flushed by meltwater, through a process termed preferential elution (Brimblecombe *et al.* 1987;
 981 Davies *et al.* 1987). Some studies have shown that sodium is removed at a similar rate to
 982 chloride and is the least mobile cation (Brimblecombe *et al.* 1985; Tsiouris *et al.* 1985;
 983 Brimblecombe *et al.* 1987; Davies *et al.* 1987), which was been attributed to the role of sea salt
 984 in atmospheric condensation by Tsiouris *et al.* (1985) but could also be related to adsorption
 985 effects (Davies *et al.* 1987). These early works were validated by a recent study which was able
 986 to quantify the ion exclusion rates governing the process of preferential elution (Costa *et al.*
 987 2020).

988 **TABLE 4.** Fractionation reported in samples of sea ice and marine ice. Enrichment (+) and
 989 depletion (–) is taken in reference to what is observed in seawater. Where the fractionation is
 990 described as equal (=), the relative composition is considered to be within the uncertainty of
 991 seawater. Where the fractionation is described as (+/–), some ice cores analyzed in the study
 992 were enriched whereas others were depleted depending on sampling location. Where the
 993 fractionation is described as (=/–), the samples broadly suggested relative depletion, but the
 994 signal was not consistent across all depths. The fractionation presented for Maus *et al.* (2011)
 995 corresponds to that of the bulk ice. The marine ice sample in Warren *et al.* (1993) corresponds to
 996 the basal ice from Amery Ice Shelf. Ice type follows the same coding described in Fig. 4 (CS:
 997 Congelation Sea Ice, M: Marine Ice).

Ice Type	Ca/Cl	K/Cl	SO ₄ /Cl	Na/Cl	Mg/Cl	Source
CS	–	–	+	=	+	Addison (1977)
CS	N/A	N/A	+/–	N/A	N/A	Reeburgh and Springer-Young (1983)
CS	–	N/A	+/–	N/A	N/A	Anderson and Jones (1985)
CS	=	–	=	=	+	Meese (1989)
CS	=	N/A	–	=	=	Gjessing <i>et al.</i> (1993)
CS	+	–	+	=	+	Granskog <i>et al.</i> (2004)
CS	=	–	–	+	–	Maus <i>et al.</i> (2011)
M	=	+	–	=	–	Warren <i>et al.</i> (1993)
M	=/–	=/–	–	–	–	Moore <i>et al.</i> (1994)
M	N/A	N/A	N/A	N/A	–	Koch <i>et al.</i> (2015)

998

999 These studies of terrestrial ice fractionation allow us to identify the processes that may alter the
1000 chemical fingerprint of the sub-ice oceans of Europa and Enceladus in their ice shells:
1001 differential diffusion and flushing by meltwater. An ice shell that entrains salt through the
1002 entrapment of brine pockets should initially be representative of the underlying ocean. This is
1003 also true for locations where frazil ice accretion occurs, although there will be some chloride
1004 enrichment that will decrease with depth, inversely correlated to salinity and brine volume
1005 fraction. If permeable brine networks remain stable over geologic time, differential diffusion
1006 may result in a relative enrichment in magnesium and depletion in potassium. This diffusion can
1007 still occur through the ice crystals in the absence of brine networks, although far less efficiently
1008 (Price 2000). The presence of magnesium in the ice shell supports the hypothesis put forth by
1009 Brown and Hand (2013) that magnesium salts from the ocean contribute to the radiolytic
1010 formation of magnesium sulfate salts at the surface of Europa. The presence of sulfate salts at
1011 surface of the ice shell is not necessarily incompatible with their early precipitation. If the ice
1012 becomes impermeable at a temperature above which any cryohydrates precipitate, then the
1013 composition of the ice should not differ significantly from that of the sub-ice ocean. If
1014 cryohydrates were to precipitate in a permeable medium, there is the potential that flushing from
1015 melt could remove these impurities from the ice, assuming brine veins were large enough to
1016 transport the minerals. In the case where a planar microstructural ice-water interface remains
1017 stable at very low growth velocities, only impurities which are soluble in the ice lattice, such as
1018 chloride, would be incorporated in the ice shell. A similar mechanism to generate an ice shell
1019 dominated by chloride is by continuous flushing of interstitial impurities by meltwater. In the
1020 case where all brine is drained from the ice shell, chloride could still be preserved within the ice
1021 lattice. This indicates that although chloride salts have been observed on the surface and are
1022 correlated with endogenous features (Trumbo *et al.* 2019), this does not necessarily imply that
1023 the ocean is dominantly composed of chloride salts. Furthermore, the association of chloride
1024 with resurfacing features is compatible with the near-surface injection of a chloride-rich brine,
1025 where sulfate minerals remain in the subsurface, consistent with the hypothesis of Schmidt *et al.*
1026 (2011) for chaos terrain formation and evolution. Vance *et al.* (2019) also suggest that an ocean
1027 rich in sulfates may not be reflected in Europa's surface composition and attribute this to
1028 fractional crystallization (i.e., sulfate minerals precipitate out of solution earlier than chloride
1029 minerals). The drainage and subsequent refreezing of melt will likely play an important role in
1030 redistributing sulfate in the ice shell, generating regions of local sulfate depletion and
1031 enrichment, respectively (Gjessing *et al.* 1993; Maus *et al.* 2011).

1032

1033 6.3. Astrobiological Implications

1034 Constraining the detailed physical structure and chemical characteristics of planetary ices has
1035 important implications for potential ice-ocean habitats and their ability to retain biosignatures. In
1036 icy world systems (e.g., Europa, Enceladus), the stratigraphic and structural evolution of the ice
1037 shell, including porosity, temperature, and chemistry, will determine the spatial habitability of
1038 the respective cryosphere and determine the preservation/degradation of biosignatures as they are
1039 transported through the ice shell (Schmidt 2020). Water activity, the availability of water in an
1040 environment (Grant 2004), is an important metric which governs the ability for organisms to

1041 grow and reproduce (Stevenson *et al.* 2015). Water activity strongly influences the ability of
1042 organisms to persist in extreme environments such as hypersaline brines on Earth and the surface
1043 of Mars (Oren 2008; Tosca *et al.* 2008).

1044 Liquid vein networks and brine pockets are important habitats in both sea ice and glacial ice on
1045 Earth (Price 2000; Price 2007; Price 2009). Although the brine channels that form in sea ice are
1046 recognized as a significant cryosphere habitat (Loose *et al.* 2011; Arrigo 2014), the ice must
1047 maintain sufficient permeability to enable nutrient exchange in support of maintaining these
1048 habitats. For this reason the cool, impermeable sea ice interior is considered to be a less
1049 favorable environment for organisms relative to the ice-water interface, even though the interior
1050 represents an environment where sunlight is more accessible (Arrigo 2014). Beneath glacier ice,
1051 nutrient exchange within liquid vein networks is considered important to maintaining in-ice
1052 habitats in the absence of sunlight (Price 2000; Price 2007; Price 2009). Even so, the discovery
1053 of sub-ice-shelf anemones which burrow into relatively impermeable glacial ice suggests that
1054 organisms may not be inhibited by the lack available pathways through the ice (Daly *et al.* 2013).
1055 The complex relationship between ice permeability and habitability is highlighted by studies of
1056 sea ice microorganisms that generate extracellular polysaccharide substances (EPS) (Krembs *et*
1057 *al.* 2011; Raymond 2011). Although the brine volume fraction in ice is increased in the presence
1058 of EPS, the similarly enhanced tortuosity results in a net decrease in permeability which allows
1059 brine to be retained in the ice (Ewert and Deming 2013).

1060 The ability for ice to entrain biosignatures can also be examined independently from its
1061 suitability as a habitat. Studies of sea ice have shown that frazil ice can concentrate biological
1062 material through mechanical incorporation resulting from the buoyant consolidation of frazil ice
1063 crystals (Garrison *et al.* 1983; Clarke and Ackley 1984; Garrison *et al.* 1989). Frazil ice also
1064 possesses the unique ability to scavenge material as it is transported through a water column
1065 (Garrison *et al.* 1989; Reimnitz *et al.* 1993; Arrigo *et al.* 2010). A notable example of these
1066 scavenging capabilities can be observed in McMurdo Sound, where benthic fauna, mobilized by
1067 anchor ice (i.e., frazil ice that accretes at the seabed), have been found at the surface of the ice
1068 shelf (see Mager *et al.* 2013). There have not been many dedicated studies examining the
1069 incorporation of biosignatures in marine ice; however, one study of protists in the marine ice of
1070 Amery Ice Shelf revealed that these organisms were likely sourced from melting sea ice in the
1071 neighboring bay and were entrained in the ice as the meltwater was transported beneath the ice
1072 shelf (Roberts *et al.* 2006). This is significant because although marine ice did not serve as the
1073 original habitat to these organisms, it could incorporate and preserve these life forms even in the
1074 uppermost portion of the ice.

1075 On ocean worlds, radiolytically generated oxidants transported from the surface may represent a
1076 viable alternative to sunlight for sub-ice organisms (Chyba 2000). If oxidant-limited, organisms
1077 within the sub-ice ocean will preferentially inhabit the ice-ocean interface where the ice shell
1078 serves as source of oxidants. Vertical motion of the ice-water interface driven by tidal deflection
1079 of the ice shell could promote nutrient exchange by permitting an influx of ocean water into the
1080 ice interior that might replenish habitats at the ice-ocean interface, similar to the tidally-driven
1081 recharge of nutrients in sea ice (Arrigo *et al.* 1995; Arrigo and Thomas 2004). The enhanced
1082 permeability of frazil ice relative to congelation ice may translate to more efficient tidally-driven

1083 nutrient exchange at interfaces dominated by such an ice texture and thus perhaps a more
1084 favorable habitat. An impermeable ice shell interior may imply a reduced concentration of
1085 preserved biosignatures if organisms migrate with brine towards the ice-ocean interface.
1086 Alternatively, the presence of EPS might prevent the drainage of brine habitats, through altering
1087 the structure of the ice, and preserve biosignatures even as the habitat becomes progressively
1088 more depleted in nutrients over time. Even if the ice-ocean interface is not inhabited, if life is
1089 present in the source water where frazil ice forms, biosignatures will likely be entrained as the
1090 frazil rises buoyantly to accumulate and consolidate at the ice-ocean interface. Because the
1091 relatively pure frazil ice is also buoyant relative to the surrounding ice shell, it can serve as a
1092 vehicle to deliver samples towards the surface where they might be sampled by a lander.
1093 Features associated with conditions favorable to the accretion of frazil ice can thus serve as
1094 promising sites for in situ investigations searching for signs of life.

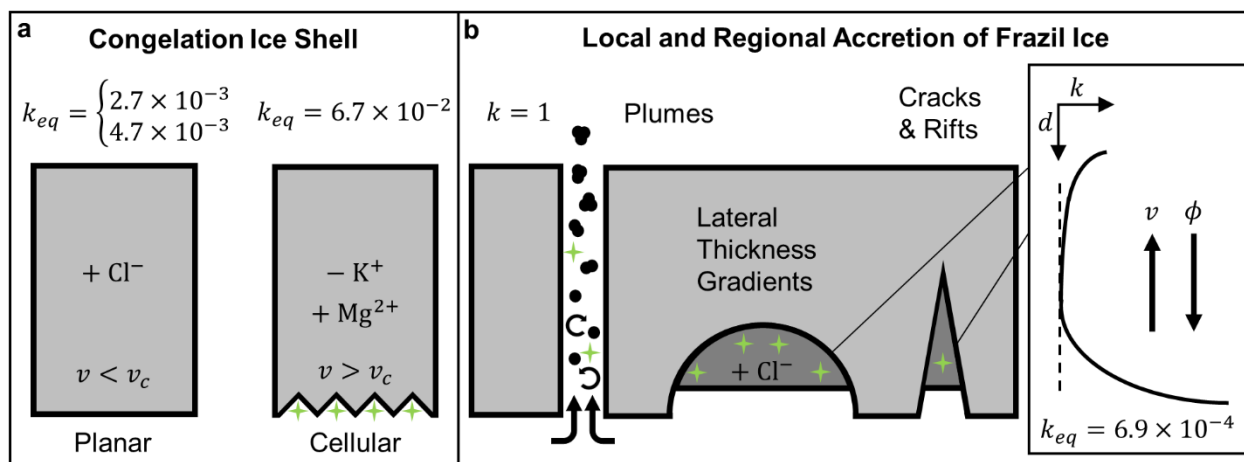
1095 An additional constraint on biological viability as well as biosignature preservation is the
1096 chaotropicity and kosmotropicity of fluids within the shell. A measure of the tendency for
1097 solutes to stabilize (kosmotropes) or destabilize (chaotropes) proteins and membranes, chao-
1098 /kosmo-tropicity impacts the habitability of brines and could limit the survivability of detectable
1099 biosignatures as they are transported through the ice shell and subjected to thermal cycling
1100 (Hallsworth *et al.* 2007; Oren 2013; Pontefract *et al.* 2017). In many naturally occurring, charge
1101 balanced systems, the presence of kosmotropes offsets the destabilizing nature of chaotropes
1102 (e.g., seawater); however, if ions are preferentially fractionated through freezing or precipitation
1103 reactions, this balance can be upset and lead to toxic chaotropic solutions (Pontefract *et al.* 2017;
1104 Brown *et al.* 2020). One notable chaotrope is chloride, suggesting that an amplified presence in
1105 an ice shell due to fractionation could challenge resident biology if concentrations are high
1106 enough (Fox-Powell *et al.* 2016). The ice salinity and fractionation thus play an important role in
1107 determining the contemporary habitability of the ice shell as well as controlling the preservation
1108 of relict biosignatures. As such, constraining the ice-ocean interface dynamics—which govern
1109 the solute entrainment within and biogeochemical evolution of the shell—is an imperative part of
1110 assessing the habitability of ice-ocean worlds and designing life detection missions (Des Marais
1111 *et al.* 2008; Council 2011; Hendrix *et al.* 2019)

1112 7. Conclusions

1113

1114 We have demonstrated that conditions at the ice-ocean interfaces of Europa and Enceladus (e.g.,
1115 composition, temperature, and pressure) could be similar to those found on Earth. We show that
1116 ice which forms in the low temperature gradient environment beneath ice shelves in Antarctica
1117 could represent a more relevant analog than sea ice. Through a systematic review of published
1118 ice core samples collected in this low temperature gradient regime, we argue that the critical
1119 factors governing the bulk salinity of ice at the low growth velocity conditions expected at the
1120 ice-ocean interfaces of icy ocean worlds are the mechanism of accreted ice formation (frazil vs.
1121 congelation) and the microstructural interface geometry (planar vs. cellular). Figure 6
1122 summarizes scenarios compatible with the formation of frazil and congelation ice beneath the ice
1123 shells of ocean worlds. Estimates of the bulk salinity associated with each mechanism are shown,

1124 expressed in terms of an effective equilibrium solute distribution coefficient, which is defined as
 1125 the ratio of the bulk ice salinity to the salinity of the source water as the growth velocity
 1126 approaches zero.
 1127



1128 **FIG. 6.** Sketch depicting bulk properties of (a) a congelation ice shell which formed in the
 1129 growth velocity regime where $k \approx k_{eq}$, (b) frazil ice accreting in local and regional features, and
 1130 (c) a profile of depth vs. solute distribution coefficient inspired by the salinity profiles of marine
 1131 ice presented in Fig. 4. v represents the growth velocity of the ice, v_c is the critical growth
 1132 velocity above which a planar ice water interface becomes unstable, k is the effective solute
 1133 distribution coefficient, d refers to the depth from the accretion interface, and ϕ is the brine
 1134 volume fraction of the ice. The $+/-$ in (a) depicts enrichment/depletion of impurities in the ice,
 1135 respectively. The plume represented in (b) shows the nucleation of frazil in the turbulent water
 1136 column as it ascends and agglomerates. The green stars represent possible locations of
 1137 biosignatures.
 1138

1139 Cooling of the ocean will promote directional freezing and the formation of a congelation ice
 1140 shell. Samples of sub-ice-shelf-congelation ice allow us to estimate the bulk salinity of an ice
 1141 shell formed through congelation growth to be $\sim 1\%$ to $\sim 10\%$ of the ocean salinity. The upper
 1142 bound effective equilibrium solute distribution coefficient derived from sub-ice-shelf congelation
 1143 ice cores, $k_{eq} = 6.7 \times 10^{-2}$, incorporates salt by the entrapment of brine pockets, which would
 1144 occur if the interface retained a cellular microstructure. The lower bound effective solute
 1145 distribution coefficient, $k_{eq} = 2.7 \times 10^{-3}$, is derived from experiments and reflects growth
 1146 conditions where a planar ice-ocean interface is stable. As such, this estimate only applies to
 1147 salts that are soluble within the ice lattice, specifically chloride. If the chlorinity of the ice
 1148 exceeds the lattice solubility limit for the lower bound distribution coefficient, any residual
 1149 chlorides will be accommodated along grain boundaries and the lower bound distribution
 1150 coefficient will increase to $k_{eq} = 4.7 \times 10^{-3}$. If fluctuations in ice shell growth rate occur that
 1151 allow for transitions in interface morphology, the bulk ice shell salinity could change by an order
 1152 of magnitude. The bulk salinity of frazil ice, which accumulates and consolidates in ice shell rifts
 1153 and basal features, is estimated to be $\sim 0.1\%$ of the ocean salinity using an effective equilibrium
 1154 solute distribution coefficient of $k_{eq} = 6.7 \times 10^{-4}$ derived from samples of marine ice.
 1155

1156 Accretion at the ice ocean interface can influence ice shell geophysical processes, composition,
1157 the distribution of habitats and biosignatures, and dielectric properties. The infilling of ice shell
1158 crevasses and troughs by frazil can serve as a mechanism for introducing thermocompositional
1159 heterogeneities into the ice shell which could promote diapirism, influence convection, and
1160 locally enhance tidal dissipation. Studies of fractionation in sea ice suggest the composition of a
1161 congelation ice shell should be approximately representative of the ocean; however, over
1162 timescales relevant to the age of the ice shell, diffusion could redistribute impurities such that the
1163 ice shell fractionation scales with both age and the mobility of impurities, provided sufficient
1164 permeability and concentration gradients are maintained. This would imply a relative enrichment
1165 in magnesium and depletion in potassium. Frazil ice accreting within basal features will become
1166 progressively more enriched in chlorides as salinity and brine volume fraction decrease towards
1167 the upper end of the ice column. Sulfates will be locally depleted and enriched where melt
1168 drainage and refreezing within the ice shell occurs, respectively. Low salinity samples of marine
1169 ice and studies of preferential elution in snow melt suggest that if interstitial salts are
1170 preferentially removed, such as through flushing of meltwater generated by tidal heating or
1171 tectonic activity, the ice shell will be enriched in chlorides. An ice shell which maintains a planar
1172 interface during freezing would also be enriched in chlorides, further supporting the idea that a
1173 chloride-dominated surface is not an unambiguous indicator of a chloride-dominated ocean. An
1174 enrichment of chlorides could challenge the habitability of brine and preservation of
1175 biosignatures within the ice shell. Locations where frazil ice forms serve as promising targets for
1176 sampling potential biosignatures entrained from the ocean given the efficient scavenging abilities
1177 of loose crystals, high permeability within the unconsolidated layer which can be recharged with
1178 oceanic material by tidal action, and the potential for thermocompositional buoyancy to deliver
1179 the material to the surface. Congelation ice may promote higher brine volume fractions relative
1180 to frazil ice at given temperature due to its higher salinity; however, if the ice is impermeable this
1181 may not translate to a sustainable habitat.

1182 The accretion of ice at the ice-ocean interface will govern the entrainment of oceanic material in
1183 the ice shell and serves as the primary filter controlling fingerprints of the ocean observable at
1184 the surface, including salinity, the relative concentration of major ionic species, as well as
1185 biosignatures. Understanding the eutectic behavior of planetary ice shells, which is directly
1186 dependent on the ice shell's composition, will improve habitability estimates for ice-ocean
1187 worlds by constraining brine volume fraction estimates as well as predictions of interstitial brine
1188 chemistry and water activity. Studies of terrestrial accreted ice can support verification and
1189 validation of planned and future missions to icy ocean worlds and serve to constrain the
1190 parameter space and detection limits for in situ and remote instrument design. Future work
1191 should leverage natural samples of these ices for improved characterization of thermal,
1192 mechanical, and electrical properties in support of these missions.

1193 **Acknowledgements**

1194 N. S. W. was supported by the G. Unger Vetlesen Foundation and the Zonta International
1195 Amelia Earhart Fellowship. K. M. S. was supported by NASA grant NNX14AR28G. D. D. B.
1196 was supported by the G. Unger Vetlesen Foundation. This work benefited from correspondence
1197 with Austin Green, John C. Moore, Lisa Craw, Lynnae Quick, Natalie Robinson, Sean Hsu,
1198 Sönke Maus, and Yosef Ashkenazy. The authors declare that they have no known competing

1199 financial interests or personal relationships which have or could be perceived to have influenced
1200 the work reported in this paper.

1201

1202 **References**

1203

1204 Addison J. R. (1977) Impurity Concentrations In Sea Ice. *Journal of Glaciology*, 18: 117-127.

1205 Anderson J., Schubert G., Jacobson R., Lau E., Moore W., and Sjogren W. (1998) Europa's
1206 differentiated internal structure: Inferences from four Galileo encounters. *Science*, 281:
1207 2019-2022.

1208 Anderson L. G., and Jones E. P. (1985) Measurements of total alkalinity, calcium, and sulfate in
1209 natural sea ice. *Journal of Geophysical Research: Oceans*, 90: 9194-9198.

1210 Arrigo K. R. (2014) Sea ice ecosystems. *Annual Review of Marine Science*, 6: 439-467.

1211 Arrigo K. R., Dieckmann G., Gosselin M., Robinson D. H., Fritsen C. H., and Sullivan C. W.
1212 (1995) High resolution study of the platelet ice ecosystem in McMurdo Sound,
1213 Antarctica: biomass, nutrient, and production profiles within a dense microalgal bloom.
1214 *Marine Ecology Progress Series*, 127: 255-268.

1215 Arrigo K. R., Mock T., and Lizotte M. P. (2010) Primary producers and sea ice. *Sea ice*, 2: 283-
1216 325.

1217 Arrigo K. R., and Thomas D. N. (2004) Large scale importance of sea ice biology in the
1218 Southern Ocean. *Antarctic Science*, 16: 471-486.

1219 Ashkenazy Y. (2019) The surface temperature of Europa. *Heliyon*, 5: e01908.

1220 Ashkenazy Y., Sayag R., and Tziperman E. (2018) Dynamics of the global meridional ice flow
1221 of Europa's icy shell. *Nature Astronomy*, 2: 43-49.

1222 Bierhaus E. B., Zahnle K., Chapman C. R., Pappalardo R., McKinnon W., and Khurana K.
1223 (2009) Europa's crater distributions and surface ages. In: *Europa*, University of Arizona
1224 Press Tucson, pp 161.

1225 Billings S. E., and Kattenhorn S. A. (2005) The great thickness debate: Ice shell thickness
1226 models for Europa and comparisons with estimates based on flexure at ridges. *Icarus*,
1227 177: 397-412.

1228 Brimblecombe P., Clegg S., Davies T., Shooter D., and Tranter M. (1987) Observations of the
1229 preferential loss of major ions from melting snow and laboratory ice. *Water Research*,
1230 21: 1279-1286.

1231 Brimblecombe P., Tranter M., Abrahams P., Blackwood I., Davies T., and Vincent C. (1985)
1232 Relocation and preferential elution of acidic solute through the snowpack of a small,
1233 remote, high-altitude Scottish catchment. *Annals of Glaciology*, 7: 141-147.

1234 Brown E. K., Buffo J. J., Grantham M., Pontefract A., Glass J., Ingall E., Doran P., Toubes-
1235 Rodrigo M., Dion-Kirschner H., and Carr C. (2020) Trapped in the Ice: An Analysis of
1236 Brines in British Columbia's Hypersaline Lakes. *LPI*: 2218.

1237 Brown M., and Hand K. (2013) Salts and radiation products on the surface of Europa. *The*
1238 *Astronomical Journal*, 145: 110.

1239 Brown M. E. (2001) Potassium in Europa's Atmosphere. *Icarus*, 151: 190-195.

1240 Bryson F. E., Nassif M., Szot P. A., Chivers C. J., Daniel N., Wiley B. E., Plattner T., Hanna A.,
1241 Tomar Y., and Rapoport S. (2020) Vertical Entry Robot for Navigating Europa (VERNE)
1242 Mission and System Design. In: *ASCEND 2020*, pp 4061.

- 1243 Buffo J., Meyer C., and Parkinson J. (2021a) Dynamics of a Solidifying Icy Satellite Shell.
1244 *Journal of Geophysical Research: Planets*: e2020JE006741.
- 1245 Buffo J., Schmidt B., and Huber C. (2018) Multiphase reactive transport and platelet ice
1246 accretion in the sea ice of McMurdo sound, Antarctica. *Journal of Geophysical Research:*
1247 *Oceans*, 123: 324-345.
- 1248 Buffo J., Schmidt B., Huber C., and Meyer C. (2021b) Characterizing the ice-ocean interface of
1249 icy worlds: A theoretical approach. *Icarus*, 360: 114318.
- 1250 Buffo J. J., Schmidt B. E., Huber C., and Walker C. C. (2020) Entrainment and Dynamics of
1251 Ocean-derived Impurities within Europa's Ice Shell. *Journal of Geophysical Research:*
1252 *Planets*.
- 1253 Burton J. A., Prim R. C., and Slichter W. P. (1953) The distribution of solute in crystals grown
1254 from the melt. Part I. Theoretical. *The journal of chemical physics*, 21: 1987-1991.
- 1255 Čadek O., Souček O., Běhouňková M., Choblet G., Tobie G., and Hron J. (2019) Long-term
1256 stability of Enceladus' uneven ice shell. *Icarus*, 319: 476-484.
- 1257 Čadek O., Tobie G., Van Hoolst T., Massé M., Choblet G., Lefèvre A., Mitri G., Baland R. M.,
1258 Běhouňková M., Bourgeois O. and others. (2016) Enceladus's internal ocean and ice shell
1259 constrained from Cassini gravity, shape, and libration data. *Geophysical Research*
1260 *Letters*, 43: 5653-5660.
- 1261 Carlson R., Anderson M., Mehlman R., and Johnson R. (2005) Distribution of hydrate on
1262 Europa: Further evidence for sulfuric acid hydrate. *Icarus*, 177: 461-471.
- 1263 Cherepanov N. V. (1964) Structure of Sea Ice of Great Thickness. *Problems of Arctic Ice*
1264 *Research*, 267: 13-18.
- 1265 Chyba C. F. (2000) Energy for microbial life on Europa. *Nature*, 403: 381-382.
- 1266 Clarke D. B., and Ackley S. F. (1984) Sea ice structure and biological activity in the Antarctic
1267 marginal ice zone. *Journal of Geophysical Research: Oceans*, 89: 2087-2095.
- 1268 Coriell S. R., McFadden G. B., and Sekerka R. F. (1985) Cellular growth during directional
1269 solidification. *Annual Review of Materials Science*, 15: 119-145.
- 1270 Costa D., Sexstone G. A., Pomeroy J. W., Campbell D. H., Clow D. W., and Mast A. (2020)
1271 Preferential elution of ionic solutes in melting snowpacks: Improving process
1272 understanding through field observations and modeling in the Rocky Mountains. *Science*
1273 *of the Total Environment*, 710: 136273.
- 1274 Council N. R. (2011) Vision and Voyages for Planetary Science in the Decade 2013-2022. The
1275 National Academies Press, Washington, DC.
- 1276 Cox G. F. N., and Weeks W. F. (1975) Brine drainage and initial salt entrapment in sodium
1277 chloride ice.
- 1278 Cox G. F. N., and Weeks W. F. (1988) Numerical simulations of the profile properties of
1279 undeformed first-year sea ice during the growth season. *Journal of Geophysical*
1280 *Research: Oceans*, 93: 12449-12460.
- 1281 Craft K., and Roberts J. Fracture formation post impact on Enceladus?
- 1282 Craft K. L., Patterson G. W., Lowell R. P., and Germanovich L. (2016) Fracturing and flow:
1283 Investigations on the formation of shallow water sills on Europa. *Icarus*, 274: 297-313.
- 1284 Craven M., Allison I., Brand R., Elcheikh A., Hunter J., Hemer M., and Donoghue S. (2004)
1285 Initial borehole results from the Amery Ice Shelf hot-water drilling project. *Annals of*
1286 *Glaciology*, 39: 531-539(9).
- 1287 Craven M., Allison I., Fricker H., and Warner R. (2009) Properties of a marine ice layer under
1288 the Amery Ice Shelf, East Antarctica. *Journal of Glaciology*, 55: 717-728(12).

- 1289 Craw L. (2020) The Ice Shelf Lasagne: Understanding the Effects of Differing Rheologies on the
 1290 Dynamics of an Ice Shelf, Abstract C015-07.AGU Fall Meeting.
- 1291 Crawford G. D., and Stevenson D. J. (1988) Gas-driven water volcanism and the resurfacing of
 1292 Europa. *Icarus*, 73: 66-79.
- 1293 Daly M., Rack F., and Zook R. (2013) *Edwardsiella andrillae*, a new species of sea anemone
 1294 from Antarctic Ice. *PloS one*, 8: e83476.
- 1295 Daly S. F. (1984) Frazil Ice Dynamics. In: *CRREL Monograph*, U.S. Army Cold Regions
 1296 Research and Engineering Laboratory, pp 56.
- 1297 Davies T., Brimblecombe P., Tranter M., Tsiouris S., Vincent C., Abrahams P., and Blackwood
 1298 I. (1987) The removal of soluble ions from melting snowpacks. In: *Seasonal snowcovers:
 1299 physics, chemistry, hydrology*, Springer, pp 337-392.
- 1300 Des Marais D. J., Nuth Iii J. A., Allamandola L. J., Boss A. P., Farmer J. D., Hoehler T. M.,
 1301 Jakosky B. M., Meadows V. S., Pohorille A., and Runnegar B. (2008) The NASA
 1302 astrobiology roadmap. *Astrobiology*, 8: 715-730.
- 1303 Dierckx M., and Tison J. L. (2013) Marine ice deformation experiments: an empirical validation
 1304 of creep parameters. *Geophysical research letters*, 40: 134-138.
- 1305 Drebuschak V. A., Drebuschak T. N., Ogienko A. G., and Yunoshev A. S. (2019)
 1306 Crystallization of sodium chloride dihydrate (hydrohalite). *Journal of Crystal Growth*,
 1307 517: 17-23.
- 1308 Eicken H. (1992) Salinity profiles of Antarctic sea ice: Field data and model results. *Journal of
 1309 Geophysical Research: Oceans*, 97: 15545-15557.
- 1310 Eicken H. (1998) Antarctic Research Series. In: *Deriving Modes and Rates of Ice Growth in the
 1311 Weddell Sea from Microstructural, Salinity, and Stable-Isotope Data*, pp 89-122.
- 1312 Eicken H. (2003) From the microscopic, to the macroscopic, to the regional scale: growth,
 1313 microstructure and properties of sea ice. *Sea ice: an introduction to its physics, chemistry,
 1314 biology and geology*: 22-81.
- 1315 Eicken H., Oerter H., Miller H., Graf W., and Kipfstuhl J. (1994) Textural characteristics and
 1316 impurity content of meteoric and marine ice in the Ronne Ice Shelf, Antarctica. *Journal
 1317 of Glaciology*, 40: 386-398.
- 1318 Ettema R., Karim M. F., and Kennedy J. F. (1984) Laboratory experiments on frazil ice growth
 1319 in supercooled water. *Cold Regions Science and Technology*, 10: 43-58.
- 1320 Ewert M., and Deming J. W. (2013) Sea ice microorganisms: Environmental constraints and
 1321 extracellular responses. *Biology*, 2: 603-628.
- 1322 Feistel R., and Wagner W. (2006) A new equation of state for H₂O ice Ih. *Journal of Physical
 1323 and Chemical Reference Data*, 35: 1021-1047.
- 1324 Fischer P. D., Brown M. E., and Hand K. P. (2015) Spatially resolved spectroscopy of Europa:
 1325 The distinct spectrum of large-scale chaos. *The Astronomical Journal*, 150: 164.
- 1326 Fitzsimons S., Mager S., Frew R., Clifford A., and Wilson G. (2012) Formation of ice-shelf
 1327 moraines by accretion of sea water and marine sediment at the southern margin of the
 1328 McMurdo Ice Shelf, Antarctica. *Annals of Glaciology*, 53: 211-220(10).
- 1329 Foldvik A., and Kvinge T. Conditional instability of sea water at the freezing point. 21: 169-174.
- 1330 Fox-Powell M. G., and Cousins C. R. (2021) Partitioning of Crystalline and Amorphous Phases
 1331 During Freezing of Simulated Enceladus Ocean Fluids. *Journal of Geophysical
 1332 Research: Planets*, 126: e2020JE006628.
- 1333 Fox-Powell M. G., Hallsworth J. E., Cousins C. R., and Cockell C. S. (2016) Ionic strength is a
 1334 barrier to the habitability of Mars. *Astrobiology*, 16: 427-442.

- 1335 Gaidos E. J., and Nimmo F. (2000) Tectonics and water on Europa. *Nature*, 405: 637-637.
- 1336 Garrison D. L., Ackley S. F., and Buck K. R. (1983) A physical mechanism for establishing algal
1337 populations in frazil ice. *Nature*, 306: 363-365.
- 1338 Garrison D. L., Close A. R., and Reimnitz E. (1989) Algae concentrated by frazil ice: evidence
1339 from laboratory experiments and field measurements. *Antarctic Science*, 1: 313-316.
- 1340 Geissler P. E., Greenberg R., Hoppa G., Helfenstein P., McEwen A., Pappalardo R., Tufts R.,
1341 Ockert-Bell M., Sullivan R., Greeley R. and others. (1998) Evidence for non-
1342 synchronous rotation of Europa. *Nature*, 391: 34869.
- 1343 Gjessing Y., Hanssen-Bauer I., Fujii Y., Kameda T., Kamiyama K., and Kawamura T. (1993)
1344 Chemical Fractionation in Sea Ice and Glacier Ice. *Bulletin of Glacier Research*: 1-8.
- 1345 Glein C., Postberg F., and Vance S. (2018) The geochemistry of enceladus: composition and
1346 controls. *Enceladus and the Icy Moons of Saturn*, 39.
- 1347 Glein C. R., Baross J. A., and Waite Jr J. H. (2015) The pH of Enceladus' ocean. *Geochimica et*
1348 *Cosmochimica Acta*, 162: 202-219.
- 1349 Golden K. M., Ackley S. F., and Lytle V. I. (1998) The Percolation Phase Transition in Sea Ice.
1350 *Science*, 282: 2238-2241.
- 1351 Golden K. M., Eicken H., Heaton A. L., Miner J., Pringle D. J., and Zhu J. (2007) Thermal
1352 evolution of permeability and microstructure in sea ice. *Geophysical Research Letters*,
1353 34.
- 1354 Goodman J. C. (2018) Interactions Between Ocean Circulation and Topography in Icy Worlds.
1355 *LPICo*, 2085: 6048.
- 1356 Gow A. J., and Epstein S. (1972) On the use of stable isotopes to trace the origins of ice in a
1357 floating ice tongue. *Journal of Geophysical Research*, 77: 6552-6557.
- 1358 Gow A. J., and Langston D. (1977) Growth history of lake ice in relation to its stratigraphic,
1359 crystalline and mechanical structure. U.S. Army Cold Regions Research and Engineering
1360 Laboratory.
- 1361 Granskog M. A., Uusikivi J., Sequeiros A. B., and Sonninen E. (2006) Relation of ice growth
1362 rate to salt segregation during freezing of low-salinity sea water (Bothnian Bay, Baltic
1363 Sea). *Annals of Glaciology*, 44: 134-138.
- 1364 Granskog M. A., Virkkunen K., Thomas D. N., Ehn J., Kola H., and Martma T. (2004) Chemical
1365 properties of brackish water ice in the Bothnian Bay, the Baltic Sea. *Journal of*
1366 *Glaciology*, 50: 292-302.
- 1367 Grant W. (2004) Life at low water activity. *Philosophical Transactions of the Royal Society of*
1368 *London. Series B: Biological Sciences*, 359: 1249-1267.
- 1369 Greeley R., Sullivan R., Coon M. D., Geissler P. E., Tufts B. R., Head J. W., Pappalardo R. T.,
1370 and Moore J. M. (1998) Terrestrial Sea Ice Morphology: Considerations for Europa.
1371 *Icarus*, 135: 25-40.
- 1372 Green A., Montesi L., and Cooper C. (2021) The Growth of Europa's Icy Shell: Convection and
1373 Crystallization. *Journal of Geophysical Research: Planets*, 126: e2020JE006677.
- 1374 Greenberg R., Geissler P., Hoppa G., Tufts B. R., Durda D. D., Pappalardo R., Head J. W.,
1375 Greeley R., Sullivan R., and Carr M. H. (1998) Tectonic Processes on Europa: Tidal
1376 Stresses, Mechanical Response, and Visible Features. *Icarus*, 135: 64-78.
- 1377 Greene C. A., Gwyther D. E., and Blankenship D. D. (2017) Antarctic mapping tools for
1378 MATLAB. *Computers & Geosciences*, 104: 151-157.

1379 Griewank P. J., and Notz D. (2013) Insights into brine dynamics and sea ice desalination from a
1380 1-D model study of gravity drainage. *Journal of Geophysical Research: Oceans*, 118:
1381 3370-3386.

1382 Gross G., Wong P., and Humes K. (1977) Concentration dependent solute redistribution at the
1383 ice–water phase boundary. III. Spontaneous convection. Chloride solutions. *The Journal*
1384 *of Chemical Physics*, 67: 5264-5274.

1385 Grothe S., Hughes K., and Langhorne P. (2014) 22nd IAHR International Symposium on Ice.
1386 Hallsworth J. E., Yakimov M. M., Golyshin P. N., Gillion J. L. M., D'Auria G., de Lima Alves
1387 F., La Cono V., Genovese M., McKew B. A., and Hayes S. L. (2007) Limits of life in
1388 MgCl₂-containing environments: chaotropy defines the window. *Environmental*
1389 *Microbiology*, 9: 801-813.

1390 Hammond N. P. (2020) Estimating the Magnitude of Cyclic Slip on Strike-Slip faults on Europa.
1391 *Journal of Geophysical Research: Planets*, 125: no-no.

1392 Hammond N. P., Parmentier E. M., and Barr A. C. (2018) Compaction and Melt Transport in
1393 Ammonia-Rich Ice Shells: Implications for the Evolution of Triton. *Journal of*
1394 *Geophysical Research: Planets*, 123: 3105-3118.

1395 Hand K., and Carlson R. (2015) Europa's surface color suggests an ocean rich with sodium
1396 chloride. *Geophysical Research Letters*, 42: 3174-3178.

1397 Hand K. P. (2017) Report of the Europa Lander science definition team. National Aeronautics
1398 and Space Administration.

1399 Hand K. P., and Chyba C. F. (2007) Empirical constraints on the salinity of the european ocean
1400 and implications for a thin ice shell. *Icarus*, 189: 424-438.

1401 Harrison J. D., and Tiller W. A. (1963) Ice interface morphology and texture developed during
1402 freezing. *Journal of Applied Physics*, 34: 3349-3355.

1403 Helfenstein P., and Parmentier E. M. (1985) Patterns of fracture and tidal stresses due to
1404 nonsynchronous rotation: Implications for fracturing on Europa. *Icarus*, 61: 175-184.

1405 Hemingway D. J., and Mittal T. (2019) Enceladus's ice shell structure as a window on internal
1406 heat production. *Icarus*, 332: 111-131.

1407 Hemingway D. J., Rudolph M. L., and Manga M. (2020) Cascading parallel fractures on
1408 Enceladus. *Nature Astronomy*, 4: 234-239.

1409 Hendrix A. R., Hurford T. A., Barge L. M., Bland M. T., Bowman J. S., Brinckerhoff W., Buratti
1410 B. J., Cable M. L., Castillo-Rogez J., and Collins G. C. (2019) The NASA roadmap to
1411 ocean worlds. *Astrobiology*, 19: 1-27.

1412 Hesse M. A., Jordan J. S., Vance S. D., and McCarthy C. (2020) Oxidant Transport Through
1413 Europa's Ice Shell by Brine Drainage from Chaotic Terrains. *LPI*: 3073.

1414 Holland P. R., Corr H. F. J., Vaughan D. G., Jenkins A., and Skvarca P. (2009) Marine ice in
1415 Larsen Ice Shelf. *Geophysical Research Letters*, 36.

1416 Hoppa G. (1999) Strike–Slip Faults on Europa: Global Shear Patterns Driven by Tidal Stress.
1417 *Icarus*, 141: 287-298.

1418 Hoppa G., Greenberg R., Tufts B. R., Geissler P., Phillips C., and Milazzo M. (2000)
1419 Distribution of strike-slip faults on Europa. *Journal of Geophysical Research: Planets*,
1420 105: 22617-22627.

1421 Hoppmann M., Richter M. E., Smith I. J., Jendersie S., Langhorne P. J., Thomas D. N., and
1422 Dieckmann G. (2020) Platelet ice, the Southern Ocean's hidden ice: a review. *Annals of*
1423 *Glaciology*, 62.

- 1424 Howell S. M. (2021) The Likely Thickness of Europa's Icy Shell. *The Planetary Science*
1425 *Journal*, 2: 129.
- 1426 Howell S. M., and Pappalardo R. T. (2018) Band Formation and Ocean-Surface Interaction on
1427 Europa and Ganymede. *Geophysical Research Letters*, 45: 4701-4709.
- 1428 Hsu H.-W., Postberg F., Sekine Y., Shibuya T., Kempf S., Horányi M., Juhász A., Altobelli N.,
1429 Suzuki K., and Masaki Y. (2015) Ongoing hydrothermal activities within Enceladus.
1430 *Nature*, 519: 207-210.
- 1431 Hunke E. C., Notz D., Turner A. K., and Vancoppenolle M. (2011) The multiphase physics of
1432 sea ice: A review. *Cryosphere*, 5: 989-1009.
- 1433 Hurford T. A., Helfenstein P., Hoppa G. V., Greenberg R., and Bills B. G. (2007) Eruptions
1434 arising from tidally controlled periodic openings of rifts on Enceladus. *Nature*, 447: 292-
1435 294.
- 1436 Iess L., Stevenson D. J., Parisi M., Hemingway D., Jacobson R. A., Lunine J. I., Nimmo F.,
1437 Armstrong J. W., Asmar S. W., and Ducci M. (2014) The gravity field and interior
1438 structure of Enceladus. *Science*, 344: 78-80.
- 1439 Jackson K. A. (2004) Constitutional supercooling surface roughening. *Journal of Crystal*
1440 *Growth*, 264: 519-529.
- 1441 Jansen D., Luckman A., Kulesa B., Holland P. R., and King E. C. (2013) Marine ice formation
1442 in a suture zone on the Larsen C Ice Shelf and its influence on ice shelf dynamics.
1443 *Journal of Geophysical Research: Earth Surface*, 118: 1628-1640.
- 1444 Jia X., Kivelson M. G., Khurana K. K., and Kurth W. S. (2018) Evidence of a plume on Europa
1445 from Galileo magnetic and plasma wave signatures. *Nature Astronomy*, 2: 459-464.
- 1446 Johnston S. A., and Montési L. G. J. (2017) The impact of a pressurized regional sea or global
1447 ocean on stresses on Enceladus. *Journal of Geophysical Research: Planets*, 122: 1258-
1448 1275.
- 1449 Kalousová K., Souček O., Tobie G., Choblet G., and Čadek O. (2014) Ice melting and downward
1450 transport of meltwater by two-phase flow in Europa's ice shell. *Journal of Geophysical*
1451 *Research: Planets*, 119: 532-549.
- 1452 Kamata S., and Nimmo F. (2017) Interior thermal state of Enceladus inferred from the
1453 viscoelastic state of the ice shell. *Icarus*, 284: 387-393.
- 1454 Kang W., Mittal T., Bire S., Campin J.-M., and Marshall J. (2021) How does salinity shape
1455 ocean circulation and ice geometry on Enceladus and other icy satellites? *arXiv preprint*
1456 *arXiv:2104.07008*.
- 1457 Kargel J. S. (1991) Brine volcanism and the interior structures of asteroids and icy satellites.
1458 *Icarus*, 94: 368-390.
- 1459 Kargel J. S., Kaye J. Z., Head Iii J. W., Marion G. M., Sassen R., Crowley J. K., Ballesteros O.
1460 P., Grant S. A., and Hogenboom D. L. (2000) Europa's crust and ocean: origin,
1461 composition, and the prospects for life. *Icarus*, 148: 226-265.
- 1462 Khazendar A., and Jenkins A. (2003) A model of marine ice formation within Antarctic ice shelf
1463 rifts. *Journal of Geophysical Research*, 108.
- 1464 Khazendar A., Rignot E., and Larour E. (2009) Roles of marine ice, rheology, and fracture in the
1465 flow and stability of the Brunt/Stancomb-Wills Ice Shelf. *Journal of Geophysical*
1466 *Research: Earth Surface*, 114.
- 1467 Khazendar A., Tison J. L., Stenni B., Dini M., and Bondesan A. (2001) Significant marine-ice
1468 accumulation in the ablation zone beneath an Antarctic ice shelf. *Journal of Glaciology*,
1469 47: 359-368.

- 1470 Kite E. S., and Rubin A. M. (2016) Sustained eruptions on Enceladus explained by turbulent
1471 dissipation in tiger stripes. *Proceedings of the National Academy of Sciences*, 113: 3972-
1472 3975.
- 1473 Koch I., Fitzsimons S., Samyn D., and Tison J.-L. (2015) Marine ice recycling at the southern
1474 McMurdo Ice Shelf, Antarctica. *Journal of Glaciology*, 61: 689-701(13).
- 1475 Krembs C., Eicken H., and Deming J. W. (2011) Exopolymer alteration of physical properties of
1476 sea ice and implications for ice habitability and biogeochemistry in a warmer Arctic.
1477 *Proceedings of the National Academy of Sciences*, 108: 3653-3658.
- 1478 Kulesa B., Jansen D., Luckman A. J., King E. C., and Sammonds P. R. (2014) Marine ice
1479 regulates the future stability of a large Antarctic ice shelf. *Nature communications*, 5: 1-7.
- 1480 Kvajić G., and Brajović V. (1971) Anisotropic segregation of (K⁺) by dendritic ice crystals.
1481 *Journal of Crystal Growth*, 11: 73-76.
- 1482 Langhorne P. J., and Robinson W. H. (1986) Alignment of crystals in sea ice due to fluid motion.
1483 *Cold Regions Science and Technology*, 12: 197-214.
- 1484 Lee S., Pappalardo R. T., and Makris N. C. (2005) Mechanics of tidally driven fractures in
1485 Europa's ice shell. *Icarus*, 177: 367-379.
- 1486 Legendre L., Aota M., Shirasawa K., Martineau M.-J., and Ishikawa M. (1991) Crystallographic
1487 structure of sea ice along a salinity gradient and environmental control of microalgae in
1488 the brine cells. *Journal of Marine Systems*, 2: 347-357.
- 1489 Leliwa-Kopystyński J., Maruyama M., and Nakajima T. (2002) The water–ammonia phase
1490 diagram up to 300 MPa: Application to icy satellites. *Icarus*, 159: 518-528.
- 1491 Leppäranta M. (2015) Structure and Properties of Lake Ice. In: *Freezing of Lakes and the*
1492 *Evolution of their Ice Cover*. edited by M Leppärantas, Springer Berlin Heidelberg,
1493 Berlin, Heidelberg, pp 51-90.
- 1494 Lewis E. L., and Perkin R. G. (1981) The Practical Salinity Scale 1978: conversion of existing
1495 data. *Deep Sea Research Part A. Oceanographic Research Papers*, 28: 307-328.
- 1496 Lewis E. L., and Perkin R. G. (1986) Ice pumps and their rates. *Journal of Geophysical*
1497 *Research: Oceans (1978–2012)*, 91: 11756-11762.
- 1498 Lior N. (1996) Freezing. In: *Heat Transfer and Fluid Flow Data Books*, Genium Publishing
1499 Corp.
- 1500 Lipenkov V. Y., Polyakova E., and Ekaykin A. (2015) Regularities of congelation ice
1501 development in subglacial Lake Vostok. *Ice and Snow*, 52: 65-77.
- 1502 Lobo A. H., Thompson A. F., Vance S. D., and Tharimena S. (2021) A pole-to-equator ocean
1503 overturning circulation on Enceladus. *Nature Geoscience*, 14: 185-189.
- 1504 Lofgren G., and Weeks W. F. (1969) Effect of growth parameters on substructure spacing in
1505 NaCl ice crystals. *Journal of Glaciology*, 8: 153-164.
- 1506 Loose B., Miller L. A., Elliott S., and Papakyriakou T. (2011) Sea ice biogeochemistry and
1507 material transport across the frozen interface. *Oceanography*, 24: 202-218.
- 1508 Mager S. M., Smith I. J., Kempema E. W., Thomson B. J., and Leonard G. H. (2013) Anchor ice
1509 in polar oceans. *Progress in Physical Geography*, 37: 468-483.
- 1510 Manga M., and Wang C. Y. (2007) Pressurized oceans and the eruption of liquid water on
1511 Europa and Enceladus. *Geophysical Research Letters*, 34.
- 1512 Martin A., and McMinn A. (2018) Sea ice, extremophiles and life on extra-terrestrial ocean
1513 worlds. *International Journal of Astrobiology*, 17: 1-16.
- 1514 Maus S. (2006) The planar-cellular transition during freezing of natural waters. 11th International
1515 Conference on the Physics and Chemistry of Ice.

- 1516 Maus S. (2007) On brine entrapment in sea ice: morphological stability, microstructure and
1517 convection. Logos-Verlag.
- 1518 Maus S. (2020) The plate spacing of sea ice. *Annals of Glaciology*, 82.
- 1519 Maus S., Müller S., Büttner J., Brütsch S., Huthwelker T., Schwikowski M., Enzmann F., and
1520 Vähätö A. (2011) Ion fractionation in young sea ice from Kongsfjorden, Svalbard.
1521 *Annals of Glaciology*, 52: 301-310.
- 1522 McCord T., Hansen G., Fanale F., Carlson R., Matson D., Johnson T., Smythe W., Crowley J.,
1523 Martin P., and Ocampo A. (1998) Salts on Europa's surface detected by Galileo's near
1524 infrared mapping spectrometer. *Science*, 280: 1242-1245.
- 1525 McCord T. B., Hansen G. B., Matson D. L., Johnson T. V., Crowley J. K., Fanale F. P., Carlson
1526 R. W., Smythe W. D., Martin P. D., and Hibbitts C. A. (1999) Hydrated salt minerals on
1527 Europa's surface from the Galileo near-infrared mapping spectrometer (NIMS)
1528 investigation. *Journal of Geophysical Research: Planets*, 104: 11827-11851.
- 1529 McCord T. B., Teeter G., Hansen G. B., Sieger M. T., and Orlando T. M. (2002) Brines exposed
1530 to Europa surface conditions. *Journal of Geophysical Research: Planets*, 107: 4-1-4-6.
- 1531 McGrath D., Steffen K., Holland P. R., Scambos T., Rajaram H., Abdalati W., and Rignot E.
1532 (2014) The structure and effect of suture zones in the Larsen C Ice Shelf, Antarctica.
1533 *Journal of Geophysical Research: Earth Surface*, 119: 588-602.
- 1534 McKinnon W. B. (2015) Effect of Enceladus's rapid synchronous spin on interpretation of
1535 Cassini gravity. *Geophysical Research Letters*, 42: 2137-2143.
- 1536 Meese D. A. (1989) The chemical and structural properties of sea ice in the southern Beaufort
1537 Sea. In: *CRREL Report*, U.S. Army Cold Regions Research and Engineering Laboratory,
1538 pp 144.
- 1539 Melnikov I. (1995) An in situ experimental study of young sea ice formation on an Antarctic
1540 lead. *Journal of Geophysical Research: Oceans*, 100: 4673-4680.
- 1541 Melwani Daswani M., Vance S. D., Mayne M. J., and Glein C. R. (2021) A metamorphic origin
1542 for Europa's ocean. *Geophysical Research Letters*, 48: e2021GL094143.
- 1543 Michaut C., and Manga M. (2014) Domes, pits, and small chaos on Europa produced by water
1544 sills. *Journal of Geophysical Research: Planets*, 119: 550-573.
- 1545 Millero F. J., Feistel R., Wright D. G., and McDougall T. J. (2008) The composition of Standard
1546 Seawater and the definition of the Reference-Composition Salinity Scale. *Deep Sea
1547 Research Part I: Oceanographic Research Papers*, 55: 50-72.
- 1548 Mitri G., and Showman A. P. (2005) Convective–conductive transitions and sensitivity of a
1549 convecting ice shell to perturbations in heat flux and tidal-heating rate: Implications for
1550 Europa. *Icarus*, 177: 447-460.
- 1551 Moore J. C., Reid A. P., and Kipfstuhl J. (1994) Microstructure and electrical properties of
1552 marine ice and its relationship to meteoric ice and sea ice. *Journal of Geophysical
1553 Research: Oceans (1978–2012)*, 99: 5171-5180.
- 1554 Morgan V. I. (1972) Oxygen Isotope Evidence for Bottom Freezing on the Amery Ice Shelf.
1555 *Nature*, 238: 393-394.
- 1556 Mullins W. W., and Sekerka R. F. (1964) Stability of a planar interface during solidification of a
1557 dilute binary alloy. *Journal of applied physics*, 35: 444-451.
- 1558 Nagashima K., and Furukawa Y. (1997) Solute distribution in front of an ice/water interface
1559 during directional growth of ice crystals and its relationship to interfacial patterns. *The
1560 Journal of Physical Chemistry B*, 101: 6174-6176.

- 1561 Nakawo M., and Sinha N. K. (1981) Growth Rate and Salinity Profile of First-Year Sea Ice in
1562 the High Arctic. *Journal of Glaciology*, 27: 315-330.
- 1563 Neal C. S. (1979) The Dynamics of the Ross Ice Shelf Revealed by Radio Echo-Sounding.
1564 *Journal of Glaciology*, 24: 295-307.
- 1565 Nimmo F. (2004a) Non-Newtonian topographic relaxation on Europa. *Icarus*, 168: 205-208.
- 1566 Nimmo F. (2004b) Stresses generated in cooling viscoelastic ice shells: Application to Europa.
1567 *Journal of Geophysical Research: Planets*, 109.
- 1568 Nimmo F., and Bills B. G. (2010) Shell thickness variations and the long-wavelength topography
1569 of Titan. *Icarus*, 208: 896-904.
- 1570 Nimmo F., and Gaidos E. (2002) Strike-slip motion and double ridge formation on Europa.
1571 *Journal of Geophysical Research: Planets*, 107: 5-1-5-8.
- 1572 Nimmo F., Thomas P. C., Pappalardo R. T., and Moore W. B. (2007) The global shape of
1573 Europa: Constraints on lateral shell thickness variations. *Icarus*, 191: 183-192.
- 1574 Notz D., and Worster M. G. (2009) Desalination processes of sea ice revisited. *Journal of*
1575 *Geophysical Research*, 114.
- 1576 Oerter H., Kipfstuhl J., Determann J., Miller H., Wagenbach D., Minikin A., and Graft W.
1577 (1992) Evidence for basal marine ice in the Filchner–Ronne ice shelf. *Nature*, 358:
1578 358399a0.
- 1579 Ojakangas G., and Stevenson D. (1989) Thermal state of an ice shell on Europa. *Icarus*, 81: 220-
1580 241.
- 1581 Oren A. (2008) Microbial life at high salt concentrations: phylogenetic and metabolic diversity.
1582 *Saline systems*, 4: 2.
- 1583 Oren A. (2013) Life in magnesium-and calcium-rich hypersaline environments: salt stress by
1584 chaotropic ions. In: *Polyextremophiles*, Springer, pp 215-232.
- 1585 Osterkamp T. E. (1977) Frazil-Ice Nucleation by Mass-Exchange Processes at the Air-Water
1586 Interface. *Journal of Glaciology*, 19: 619-627.
- 1587 Osterkamp T. E., and Weber A. H. (1970) Electrical phenomena accompanying the phase change
1588 of dilute KCl solutions into single crystals of ice. *Journal of Glaciology*, 9: 269-277.
- 1589 Pappalardo R., Head J., Greeley R., Sullivan R., Pilcher C., Schubert G., Moore W., Carr M.,
1590 Moore J., and Belton M. (1998) Geological evidence for solid-state convection in
1591 Europa's ice shell. *Nature*, 391: 365-368.
- 1592 Pappalardo R. T., and Barr A. C. (2004) The origin of domes on Europa: The role of thermally
1593 induced compositional diapirism. *Geophysical Research Letters*, 31.
- 1594 Patthoff D. A., Kattenhorn S. A., and Cooper C. M. (2019) Implications of nonsynchronous
1595 rotation on the deformational history and ice shell properties in the south polar terrain of
1596 Enceladus. *Icarus*, 321: 445-457.
- 1597 Pattyn F., Matsuoka K., Callens D., Conway H., Depoorter M., Docquier D., Hubbard B., Samyn
1598 D., and Tison J. L. (2012) Melting and refreezing beneath Roi Baudouin Ice Shelf (East
1599 Antarctica) inferred from radar, GPS, and ice core data. *Journal of Geophysical*
1600 *Research: Earth Surface*, 117.
- 1601 Peddinti D. A., and McNamara A. K. (2015) Material transport across Europa's ice shell.
1602 *Geophysical Research Letters*, 42: 4288-4293.
- 1603 Peddinti D. A., and McNamara A. K. (2019) Dynamical investigation of a thickening ice-shell:
1604 Implications for the icy moon Europa. *Icarus*, 329: 251-269.
- 1605 Petrich C., and Eicken H. (2017) Overview of sea ice growth and properties. In: *Sea Ice*. edited
1606 by DN Thomass, John Wiley & Sons, pp 1-41.

- 1607 Petrich C., Langhorne P., and Eicken H. (2011) Modeled Bulk Salinity of Growing First-Year
 1608 Sea Ice and Implications for Ice Properties in Spring. International Conference on Port
 1609 and Ocean Engineering under Arctic Conditions, Montreal, Canada.
- 1610 Petrich C., Langhorne P. J., and Sun Z. F. (2006) Modelling the interrelationships between
 1611 permeability, effective porosity and total porosity in sea ice. *Cold Regions Science and
 1612 Technology*, 44: 131-144.
- 1613 Pillay V., Gärtner R. S., Himawan C., Seckler M. M., Lewis A. E., and Witkamp G.-J. (2005)
 1614 MgSO₄+ H₂O System at Eutectic Conditions and Thermodynamic Solubility Products of
 1615 MgSO₄⊙ 12H₂O (s) and MgSO₄⊙ 7H₂O (s). *Journal of Chemical & Engineering
 1616 Data*, 50: 551-555.
- 1617 Pontefract A., Zhu T. F., Walker V. K., Hepburn H., Lui C., Zuber M. T., Ruvkun G., and Carr
 1618 C. E. (2017) Microbial diversity in a hypersaline sulfate lake: a terrestrial analog of
 1619 ancient Mars. *Frontiers in microbiology*, 8: 1819.
- 1620 Postberg F., Clark R. N., Hansen C. J., Coates A. J., Dalle Ore C. M., Scipioni F., Hedman M.
 1621 M., and Waite J. H. (2018) Plume and surface composition of Enceladus. *Enceladus and
 1622 the Icy Moons of Saturn*: 129-162.
- 1623 Postberg F., Kempf S., Schmidt J., Brilliantov N., Beinsen A., Abel B., Buck U., and Srama R.
 1624 (2009) Sodium salts in E-ring ice grains from an ocean below the surface of Enceladus.
 1625 *Nature*, 459: 1098-1101.
- 1626 Postberg F., Schmidt J., Hillier J., Kempf S., and Srama R. (2011) A salt-water reservoir as the
 1627 source of a compositionally stratified plume on Enceladus. *Nature*, 474: 620-2.
- 1628 Price P. B. (2000) A habitat for psychrophiles in deep Antarctic ice. *Proceedings of the National
 1629 Academy of Sciences*, 97: 1247-1251.
- 1630 Price P. B. (2007) Microbial life in glacial ice and implications for a cold origin of life. *FEMS
 1631 Microbiology Ecology*, 59: 217-231.
- 1632 Price P. B. (2009) Microbial genesis, life and death in glacial ice. *Canadian journal of
 1633 microbiology*, 55: 1-11.
- 1634 Prockter L. M., Pappalardo R. T., and Head Iii J. W. (2000) Strike-slip duplexing on Jupiter's icy
 1635 moon Europa. *Journal of Geophysical Research: Planets*, 105: 9483-9488.
- 1636 Quick L. C., and Marsh B. D. (2015) Constraining the thickness of Europa's water-ice shell:
 1637 insights from tidal dissipation and conductive cooling. *Icarus*, 253: 16-24.
- 1638 Raymond J. A. (2011) Algal ice-binding proteins change the structure of sea ice. *Proceedings of
 1639 the National Academy of Sciences*, 108: E198-E198.
- 1640 Reeburgh W. S., and Springer-Young M. (1983) New measurements of sulfate and chlorinity in
 1641 natural sea ice. *Journal of Geophysical Research: Oceans*, 88: 2959-2966.
- 1642 Reimnitz E., Clayton J. R., Kempema E. W., Payne J. R., and Weber W. S. (1993) Interaction of
 1643 rising frazil with suspended particles: tank experiments with applications to nature. *Cold
 1644 Regions Science and Technology*, 21: 117-135.
- 1645 Rhoden A. R., Hurford T. A., and Manga M. (2011) Strike-slip fault patterns on Europa:
 1646 Obliquity or polar wander? *Icarus*, 211: 636-647.
- 1647 Rhoden A. R., Wurman G., Huff E. M., Manga M., and Hurford T. A. (2012) Shell tectonics: A
 1648 mechanical model for strike-slip displacement on Europa. *Icarus*, 218: 297-307.
- 1649 Roberts D., Craven M., Cai M., Allison I., and Nash G. (2006) Protists in the marine ice of the
 1650 Amery Ice Shelf, East Antarctica. *Polar Biology*, 30: 143-153.

- 1651 Roberts J. H., and Nimmo F. (2008) Tidal heating and the long-term stability of a subsurface
1652 ocean on Enceladus. *Icarus*, 194: 675-689.
- 1653 Robinson N. J., Grant B. S., Stevens C. L., Stewart C. L., and Williams M. J. M. (2019)
1654 Oceanographic observations in supercooled water: Protocols for mitigation of
1655 measurement errors in profiling and moored sampling. *Cold Regions Science and
1656 Technology*: 102954.
- 1657 Rudolph M. L., and Manga M. (2009) Fracture penetration in planetary ice shells. *Icarus*, 199:
1658 536-541.
- 1659 Russell M. J., Murray A. E., and Hand K. P. (2017) The possible emergence of life and
1660 differentiation of a shallow biosphere on irradiated icy worlds: the example of Europa.
1661 *Astrobiology*, 17: 1265-1273.
- 1662 Rutter J. W., and Chalmers B. (1953) A prismatic substructure formed during solidification of
1663 metals. *Canadian Journal of Physics*, 31: 15-39.
- 1664 Schenk P., Matsuyama I., and Nimmo F. (2008) True polar wander on Europa from global-scale
1665 small-circle depressions. *Nature*, 453: 368.
- 1666 Schilling N., Khurana K. K., and Kivelson M. G. (2004) Limits on an intrinsic dipole moment in
1667 Europa. *Journal of Geophysical Research: Planets (1991–2012)*, 109.
- 1668 Schilling N., Neubauer F. M., and Saur J. (2007) Time-varying interaction of Europa with the
1669 jovian magnetosphere: Constraints on the conductivity of Europa's subsurface ocean.
1670 *Icarus*, 192: 41-55.
- 1671 Schmidt B. E. (2020) The Astrobiology of Europa and the Jovian System. *Planetary
1672 Astrobiology*: 185.
- 1673 Schmidt B. E., Blankenship D. D., Patterson G. W., and Schenk P. M. (2011) Active formation
1674 of 'chaos terrain' over shallow subsurface water on Europa. *Nature*, 479: 502.
- 1675 Seidensticker R. G. (1972) Partitioning of HCl in the water-ice system. *The Journal of Chemical
1676 Physics*, 56: 2853-2857.
- 1677 Sekerka R. F., Coriell S. R., and McFadden G. B. (2015) Morphological stability. In: *Handbook
1678 of Crystal Growth*, Elsevier, pp 595-630.
- 1679 Shokr M., and Sinha N. (2015) Sea ice: physics and remote sensing. John Wiley & Sons.
- 1680 Soderlund K. M. (2019) Ocean dynamics of outer solar system satellites. *Geophysical Research
1681 Letters*, 46: 8700-8710.
- 1682 Soderlund K. M., Kalousova K., Buffo J. J., Glein C. R., Goodman J. C., Mitri G., Patterson G.
1683 W., Postberg F., Rovira-Navarro M., Rückriemen T. and others. (2020) Ice-Ocean
1684 Exchange Processes in the Jovian and Saturnian Satellites. *Space Science Reviews*, 216:
1685 1-57.
- 1686 Soderlund K. M., Schmidt B. E., Wicht J., and Blankenship D. D. (2013) Ocean-driven heating
1687 of Europa's icy shell at low latitudes. *Nature Geoscience*, 7: 16-19.
- 1688 Sotin C., Head III J. W., and Tobie G. (2002) Europa: Tidal heating of upwelling thermal plumes
1689 and the origin of lenticulae and chaos melting. *Geophysical Research Letters*, 29: 74-1-
1690 74-4.
- 1691 Souchez R., Meneghel M., Tison J. L., Lorrain R., Ronveaux D., Baroni C., Lozej A., Tabacco
1692 I., and Jouzel J. (1991) Ice composition evidence of marine ice transfer along the bottom
1693 of a small Antarctic Ice Shelf. *Geophysical Research Letters*, 18: 849-852.
- 1694 Souchez R., Petit J.-R., Tison J.-L., Jouzel J., and Verbeke V. (2000) Ice formation in subglacial
1695 Lake Vostok, central Antarctica. *Earth and Planetary Science Letters*, 181: 529-538.

1696 Souchez R., Petit J. R., Jouzel J., De Angelis M., and Tison J. L. (2004) Reassessing Lake
1697 Vostok's behaviour from existing and new ice core data. *Earth and Planetary Science*
1698 *Letters*, 217: 163-170.

1699 Souchez R., Tison J. L., and Jouzel J. (1988) Deuterium concentration and growth rate of
1700 Antarctic first-year sea ice. *Geophysical research letters*, 15: 1385-1388.

1701 Sparks W. B., Schmidt B. E., McGrath M. A., Hand K. P., Spencer J. R., Cracraft M., and
1702 Deustua S. E. (2017) Active cryovolcanism on Europa? *The Astrophysical Journal*
1703 *Letters*, 839: L18.

1704 Spencer J., Nimmo F., Ingersoll A. P., Hurford T., Kite E., Rhoden A., Schmidt J., and Howett
1705 C. (2018) Plume origins and plumbing: from ocean to surface. *Enceladus and the Icy*
1706 *Moons of Saturn*: 163.

1707 Spencer J. R., Pearl J. C., Segura M., Flasar F. M., Mamoutkine A., Romani P., Buratti B. J.,
1708 Hendrix A. R., Spilker L. J., and Lopes R. M. C. (2006) Cassini Encounters Enceladus:
1709 Background and the Discovery of a South Polar Hot Spot. *Science*, 311: 1401-1405.

1710 Squyres S. W., Reynolds R. T., Cassen P. M., and Peale S. J. (1983) The evolution of Enceladus.
1711 *Icarus*, 53: 319-331.

1712 Steinbrügge G., Voigt J. R. C., Wolfenbarger N. S., Hamilton C. W., Soderlund K. M., Young D.
1713 A., Blankenship D. D., Vance S. D., and Schroeder D. M. (2020) Brine Migration and
1714 Impact-Induced Cryovolcanism on Europa. *Geophysical Research Letters*, 47:
1715 e2020GL090797.

1716 Stevenson A., Cray J. A., Williams J. P., Santos R., Sahay R., Neuenkirchen N., McClure C. D.,
1717 Grant I. R., Houghton J. D., and Quinn J. P. (2015) Is there a common water-activity
1718 limit for the three domains of life? *The ISME journal*, 9: 1333-1351.

1719 Tajeddine R., Soderlund K. M., Thomas P. C., Helfenstein P., Hedman M. M., Burns J. A., and
1720 Schenk P. M. (2017) True polar wander of Enceladus from topographic data. *Icarus*, 295:
1721 46-60.

1722 Terwilliger J. P., and Dizio S. F. (1970) Salt rejection phenomena in the freezing of saline
1723 solutions. *Chemical Engineering Science*, 25: 1331-1349.

1724 Thomas D. N. (2017) Sea ice. John Wiley & Sons.

1725 Thomas E. C., Hodyss R., Vu T. H., Johnson P. V., and Choukroun M. (2017) Composition and
1726 evolution of frozen chloride brines under the surface conditions of Europa. *ACS Earth*
1727 *and Space Chemistry*, 1: 14-23.

1728 Tison J. L., Khazendar A., and Roulin E. (2001) A two-phase approach to the simulation of the
1729 combined isotope/salinity signal of marine ice. *Journal of Geophysical Research:*
1730 *Oceans*, 106: 31387-31401.

1731 Tison J. L., Lorrain R. D., Bouzette A., Dini M., Bondesan A., and StiéVenard M. (1998)
1732 Linking Landfast Sea Ice Variability to Marine Ice Accretion at Hells Gate Ice Shelf,
1733 Ross Sea. pp 375-407.

1734 Tison J. L., Ronveaux D., and Lorrain R. D. (1993) Low salinity frazil ice generation at the base
1735 of a small Antarctic ice shelf. *Antarctic Science*, 5: 309-322.

1736 Toner J. D., Catling D. C., and Light B. (2014) The formation of supercooled brines, viscous
1737 liquids, and low-temperature perchlorate glasses in aqueous solutions relevant to Mars.
1738 *Icarus*, 233: 36-47.

1739 Tosca N. J., Knoll A. H., and McLennan S. M. (2008) Water activity and the challenge for life
1740 on early Mars. *Science*, 320: 1204-1207.

1741 Trumbo S. K., Brown M. E., and Hand K. P. (2019) Sodium chloride on the surface of Europa.
1742 *Science advances*, 5: eaaw7123.

1743 Tsiouris S., Vincent C. E., Davies T. D., and Brimblecombe P. (1985) The elution of ions
1744 through field and laboratory snowpacks. *Annals of Glaciology*, 7: 196-201.

1745 Turtle E. P., and Pierazzo E. (2001) Thickness of a European ice shell from impact crater
1746 simulations. *Science*, 294: 1326-1328.

1747 Vance S., and Goodman J. (2009) Oceanography of an ice-covered moon. *Europa*: 459-482.

1748 Vance S. D., Barge L. M., Cardoso S., and Cartwright J. (2019) Self-Assembling Ice Membranes
1749 on Europa: Brinicle Properties, Field Examples, and Possible Energetic Systems in Icy
1750 Ocean Worlds. *Astrobiology*, 19: 685-695.

1751 Vance S. D., Hand K. P., and Pappalardo R. T. (2016) Geophysical controls of chemical
1752 disequilibria in Europa. *Geophysical Research Letters*, 43: 4871-4879.

1753 Vance S. D., Journaux B., Hesse M., and Steinbrügge G. (2021a) The Salty Secrets of Icy Ocean
1754 Worlds. *Journal of Geophysical Research: Planets*, 126: e2020JE006736.

1755 Vance S. D., Styczinski M., Bills B., Cochrane C., Soderlund K., Gómez-Pérez N., and Paty C.
1756 (2021b) Magnetic induction responses of Jupiter's ocean moons including effects from
1757 adiabatic convection. *Journal of Geophysical Research: Planets*, 126: e2020JE006418.

1758 Waite J. H., Glein C. R., Perryman R. S., Teolis B. D., Magee B. A., Miller G., Grimes J., Perry
1759 M. E., Miller K. E., and Bouquet A. (2017) Cassini finds molecular hydrogen in the
1760 Enceladus plume: evidence for hydrothermal processes. *Science*, 356: 155-159.

1761 Waite J. H., Lewis W. S., Magee B. A., Lunine J. I., McKinnon W. B., Glein C. R., Mousis O.,
1762 Young D. T., Brockwell T., Westlake J. and others. (2009) Liquid water on Enceladus
1763 from observations of ammonia and 40Ar in the plume. *Nature*, 460: 487-490.

1764 Walker C. C., Bassis J. N., and Schmidt B. E. (2021) Propagation of Vertical Fractures through
1765 Planetary Ice Shells: The Role of Basal Fractures at the Ice–Ocean Interface and
1766 Proximal Cracks. *The Planetary Science Journal*, 2: 135.

1767 Walker C. C., and Schmidt B. E. (2015) Ice collapse over trapped water bodies on Enceladus and
1768 Europa. *Geophysical Research Letters*, 42: 712-719.

1769 Warren S. G., Roesler C. S., Morgan V. I., Brandt R. E., Goodwin I. D., and Allison I. (1993)
1770 Green icebergs formed by freezing of organic-rich seawater to the base of Antarctic ice
1771 shelves. *Journal of Geophysical Research: Oceans (1978–2012)*, 98: 6921-6928.

1772 Weeks W. (2010) On sea ice. University of Alaska Press.

1773 Weeks W. F., and Ackley S. F. (1986) The Growth, Structure, and Properties of Sea Ice. In:
1774 *CRREL Monograph*, U.S. Army Cold Regions Research and Engineering Laboratory, pp
1775 9-164.

1776 Weeks W. F., and Lofgren G. (1967) The effective solute distribution coefficient during the
1777 freezing of NaCl solutions. *Physics of snow and ice: Proceedings*, 1: 579-597.

1778 Wells A. J., Hitchen J. R., and Parkinson J. R. G. (2019) Mushy-layer growth and convection,
1779 with application to sea ice. *Philosophical Transactions of the Royal Society A*, 377:
1780 20180165.

1781 Wettlaufer J. S. (1992) Directional Solidification of Salt Water: Deep and Shallow Cells.
1782 *Europhysics Letters (EPL)*, 19: 337-342.

1783 Wettlaufer J. S. (1998) Introduction to crystallization phenomena in natural and artificial sea ice.
1784 *The Physics of ice covered seas, edited by: Lepparantä, M., Univ. of Helsinki, Helsinki:*
1785 105-195.

- 1786 Zeng Y., and Jansen M. F. (2021) Ocean Circulation on Enceladus with a High- versus Low-
1787 salinity Ocean. *The Planetary Science Journal*, 2: 151.
- 1788 Zimmer C., Khurana K. K., and Kivelson M. G. (2000) Subsurface Oceans on Europa and
1789 Callisto: Constraints from Galileo Magnetometer Observations. *Icarus*, 147: 329-347.
- 1790 Zolotov M. Y. (2007) An oceanic composition on early and today's Enceladus. *Geophysical*
1791 *Research Letters*, 34.
- 1792 Zolotov M. Y. (2008) Oceanic composition on Europa: Constraints from mineral
1793 solubilities. Lunar and Planetary Science Conference.
- 1794 Zolotov M. Y., and Kargel J. S. (2009) On the chemical composition of Europa's icy shell,
1795 ocean, and underlying rocks. University of Arizona Press Tucson, AZ.
- 1796 Zolotov M. Y., and Shock E. L. (2001) Composition and stability of salts on the surface of
1797 Europa and their oceanic origin. *Journal of Geophysical Research: Planets (1991–2012)*,
1798 106: 32815-32827.
- 1799 Zotikov I. A., Zagorodnov V. S., and Raikovskiy J. V. (1980) Core Drilling Through the Ross Ice
1800 Shelf (Antarctica) Confirmed Basal Freezing. *Science*, 207: 1463-1465.
- 1801